

Painting a Family Portrait of the Yellow Super- and Hypergiants in the Milky Way

I. Constraining the Distances and Luminosities

A. Kasikov^{1,2}, A. Mehner², I. Kolka¹, and A. Aret¹

¹ Tartu Observatory, University of Tartu, Observatooriumi 1, Tõravere, 61602, Estonia
e-mail: anni.kasikov@ut.ee

² European Southern Observatory, Alonso de Córdova 3107, Vitacura, Casilla 19001, Santiago de Chile, Chile

Received ; accepted

ABSTRACT

Context. Distances to evolved massive stars in the Milky Way are not well constrained by *Gaia* parallaxes due to their brightness and variability. This makes it difficult to determine their fundamental stellar parameters, such as radius or luminosity, and infer their evolutionary states.

Aims. We aim to improve the distance estimates of Yellow Hypergiants (YHGs) and Yellow Supergiants (YSGs) by identifying possible cluster and association memberships. Using these distances, we derived updated luminosities and revised their positions in the Hertzsprung-Russell diagram.

Methods. We compiled from the literature a sample of 35 luminous yellow massive stars (YHGs and the most luminous YSGs). We used *Gaia* DR3 astrometry to identify possible membership in clusters and OB associations. We derived distances by combining the parallaxes of nearby co-moving stars. We independently validated these distances by comparing the stellar radial velocities to the Galactic H α kinematic map. We combined angular diameters and effective temperature values from the literature with the new distances to estimate luminosities.

Results. We improved the distance estimates for 28 of the 35 stars through association with co-moving stellar groups. For an additional six stars, we provided distance estimates based on the H α kinematic map. For one star, the distance remains unclear. Most YSGs are members of young stellar populations, while the environments of the YHGs are more diverse, and for some of them their origin populations remain unclear. We derived updated luminosities for a subset of 20 stars. Most YHGs have luminosities above $\log L/L_\odot = 5.4$, while YSGs occupy a wider range of luminosities and the most luminous YSGs have luminosities similar to YHGs.

Key words. Stars: massive – Supergiants – Stars: distances – Methods: observational

1. Introduction

Stellar population studies of young star clusters have revealed numerous massive stars in transitional evolutionary phases (recently, e.g. Marco et al. 2025; Maíz Apellániz & Negueruela 2025). Knowledge of the surrounding stellar population and environment provides context for understanding the evolution of massive stars. Yellow Supergiants (YSGs) and the rarer, more elusive Yellow Hypergiants (YHGs) are unstable and short-lived phases on the cool side of the upper Hertzsprung-Russell (HR) diagram. YHGs are generally considered to represent a more extreme or advanced stage of evolution than typical YSGs and have been proposed as post-Red Supergiants (post-RSGs) (de Jager 1998).

The distinction between YHGs and YSGs is based on their spectroscopic characteristics: YHGs have extended atmospheres, one or more broad H α emission components, and significantly wider absorption lines compared to YSGs (de Jager 1998). Beyond using spectroscopic features to differentiate YHGs from YSGs, studies have proposed luminosity thresholds ($\log L/L_\odot > 5.2$; de Jager & Nieuwenhuijzen 1997), distinct pulsational behaviour and presence of circumstellar dust (Humphreys et al. 2023), and a high $^{12}\text{CO}/^{13}\text{CO}$ isotopic ratio (Oksala et al. 2013). Homogeneously determined observa-

tional parameters of YHGs and YSGs provide a basis for comparison with stellar evolutionary models, improving our overall understanding of evolutionary pathways of luminous yellow massive stars and their role as supernova progenitors (e.g. Aldering et al. 1994; Crockett et al. 2008; Maund et al. 2011; Tartaglia et al. 2017; Kilpatrick et al. 2017; Niu et al. 2024; Reguitti et al. 2025).

Extensive work has been done to characterise the luminous cool Supergiant populations of the Magellanic Clouds and other nearby galaxies (e.g. Martin & Humphreys 2023; Dorn-Wallenstein et al. 2023; Maravelias et al. 2025). However, in the Milky Way, studies have been hampered by uncertain distances and high extinction in the Galactic plane. In the era of *Gaia* and due to the efforts by Bailer-Jones et al. (2021), the distance estimates for many stars have improved significantly. For objects that lack reliable *Gaia* parallaxes, other indirect methods can be used to estimate distances. We combined and compared the results of two complementary methods. The first method is based on analysis of nearby stars: since many YHGs and YSGs are known or suspected members of stellar clusters or OB associations, confirming these memberships and combining the parallaxes of nearby stars (e.g. Campillay et al. 2019) can help refine their distance estimates. The second method compares the stellar radial velocities with the Galactic H α kinematics. Agreement

between these independent methods increases confidence in the derived distances.

In Sect. 2, we give an overview of the selected targets. In Sect. 3, we revisit the cluster and OB association memberships of YHGs and YSGs in the Milky Way and determine the distances to the stellar groups. In Sect. 4, we derive independent distance estimates using the H α kinematic map of the Milky Way. In Sect. 5, we combine our distance measurements with effective temperatures and angular radii from the literature to place the Milky Way YHGs and YSGs on the HR diagram. Finally, in Sect. 6, we discuss the spatial distribution and binary properties of our sample stars.

2. Sample selection

We queried Simbad for YSGs and F- and G- spectral class stars with luminosity class Ia or Iab with infrared excess ($V - K > 3$ mag). From the resulting list, we excluded objects that are identified in the literature as luminous post-asymptotic giant branch (post-AGB) stars. We also excluded stars with reliable *Gaia* DR3 parallaxes that place them closer than expected for being luminous YSGs. We added additional luminous YSGs from the literature (de Jager 1998; Mantegazza 1992; Kovtyukh et al. 2012) and included stars that have been proposed as YHG candidates: IRAS 18357-0604 (Clark et al. 2014), and HD 144812 (Kourniotis et al. 2025). The resulting 25 stars form our sample of YSGs.

We also included the well-known YHGs in the Milky Way: V509 Cas, ρ Cas, IRC +10420, HR 5171, 6 Cas, HD 96918, and the Yellow-Red Hypergiant RW Cep (de Jager 1998); IRAS 17163-3907 (Lagadec et al. 2011); HD 179821 (Hawkins et al. 1995); and [FMR2006] 15 (Figer et al. 2006). When mentioning YHGs throughout this paper, we refer to the ten stars in this list.

We are not aiming for a complete census, but rather for a representative sample of the most luminous YSGs and YHGs. The final sample of 35 objects is presented in Table 1.

3. Distances based on stellar group identification

Gaia Data Release 3 (DR3) (Gaia Collaboration et al. 2016, 2023) has provided proper motion and parallax measurements for ~ 1.3 billion sources, enabling improved determinations of distances and cluster memberships. However, *Gaia* parallaxes are subject to systematics and biases. For YHGs and YSGs, the parallax values can have large uncertainties ($> 20\%$) and, in some cases, they are even negative. A major source of error is their brightness; approximately half of our sample is brighter than $G = 6$ mag. Another source of astrometric error for cool massive stars is caused by photocentric variability due to surface convection (Chiavassa et al. 2011; Pasquato et al. 2011; El-Badry 2025). Additionally, some stars have high values of renormalised unit weight error (RUWE), indicating poor astrometric fits, which may result from an unresolved binary companion (e.g. Castro-Ginard et al. 2024) or circumstellar structure (Fitton et al. 2022).

Bailer-Jones et al. (2021) provided probabilistic distance estimates that take into account the Galactic structure and mitigate the limitations of the simple 1/parallax distance estimate. Although generally more reliable, these distance estimates still require careful interpretation. In several cases, the Bailer-Jones et al. (2021) distances disagree with the values commonly adopted in the literature (see Table 1). For stars with RUWE < 1.4 and parallax uncertainties better than 20%, the Bailer-Jones et al. (2021) distances are likely to be reliable.

To improve the distances for YHGs and YSGs with poor *Gaia* parallaxes, we explored their kinematics based on proper motions in the context of their surrounding stellar environments – nearby star clusters, OB associations, and regions hosting Young Stellar Objects (YSOs). We cross-matched several catalogues of open clusters and OB associations with *Gaia* data. Membership in such co-moving groups implies common distance.

3.1. Method

To determine possible open cluster memberships, we queried the catalogue of Hunt & Reffert (2024). We counted a YHG/YSG as a member of a cluster if its projected on-sky position is within the cluster boundaries and its proper motion is within 3σ of the cluster's mean proper motion. When reliable parallaxes are available, we also used them to confirm membership. We checked whether the stars are members of any known OB associations listed by Mel'nik & Dambis (2017). We compared the proper motions of the YHGs and YSGs with members of the OB associations in the catalogue by Chemel et al. (2022) to infer a possible affiliation. OB associations extend farther than clusters in the area projected on sky and are less tightly connected in proper motion space. We counted a YHG/YSG as affiliated with an OB association when at least 2 association members are located within a 1 deg radius on the sky and within a 0.5 mas yr $^{-1}$ radius in proper motion space. In most cases, there are significantly more stars with similar proper motion in the same sky region. We list possible cluster and OB association memberships in the "Identified cl/assoc" column of Table 1. Detailed notes for all individual stars are provided in App. A.

To estimate the group-based distance for each target, we identified stars with high-quality astrometric data belonging to the same population. Proper motions and positions are not enough to differentiate between stellar populations, another criterion is needed (e.g. colour index was used by Negueruela et al. 2022). We used the effective temperature T_{eff} from *Gaia* GSP-Phot as an additional criterion. Since we searched for co-located and co-moving populations associated with young clusters or OB associations, we limited our search to B-type and early A-type stars with effective temperatures $8\,700\text{K} < T_{\text{eff}} < 18\,000\text{K}$. This approach assumes that YSGs/YHGs are still physically associated with their birth environments. If the star has migrated or has been ejected from its birth environment, we might not be able to identify a co-moving group, and this method becomes unreliable. We followed the methodology given by Campillay et al. (2019) and Maíz Apellániz et al. (2021a,b).

We identified hot stars belonging to the neighbourhood of each YHG and YSG, combined their parallaxes, and estimated the distance to the stellar group following these steps:

1. Select hot stars with high-quality astrometry within $10'$ of the target, applying the following selection criteria: good astrometry (RUWE < 1.4); bright sources ($G < 18$ mag); reliable parallaxes (parallax/error > 5); 5-parameter astrometric solution (ASTROMETRIC_PARAMS_SOLVED=31).
2. Correct the *Gaia* proper motions for known biases affecting bright targets, following the methodology of Cantat-Gaudin & Brandt (2021).
3. Apply a proper motion cut to separate stars with similar kinematics.

4. Correct the parallaxes for *Gaia* zero point offsets (Lindegren et al. 2021a)¹.
5. Calculate the group parallax, combining the individual parallaxes and errors following the recipe given in Campillay et al. (2019), considering the external parallax uncertainty (Fabricius et al. 2021) and the angular covariance term. The systematic parallax uncertainty gives a minimum distance uncertainty of $\approx d\%$ for a star at d kpc (Maíz Apellániz et al. 2021b).
6. Convert the group parallax into a geometric distance, using the generalized gamma distribution (GGD) prior of Bailer-Jones et al. (2021)²

The range of the proper motion cut is flexible and depends on the stellar environment of each YSG in our sample. By exploring the scatter of proper motions of stars recognised as members of a single cluster in the catalogue of Hunt & Reffert (2024), we found that cluster stars typically have a dispersion in proper motion of $\sim 0.2\text{--}0.3$ mas yr^{-1} . In contrast, stars in OB associations in the catalogues of Chemel et al. (2022) and Mel’nik & Dambis (2017) are less bound, showing a proper motion dispersion of $\sim 1\text{--}2$ mas yr^{-1} (Fig. 1). Thus, depending on the stellar environments surrounding each target, the cut radius varies from 0.1 to 1.5 mas yr^{-1} .

A YSG/YHG may still belong to a stellar group even if no nearby co-moving stars are identified in our search. We estimated the limiting distance at which hot stars would still fall within our criteria. As a representative case, we considered a B3 main-sequence star with $T_{\text{eff}} = 17\,000$ K and an absolute G -band magnitude $M_G = -1.19$ mag.³ We adopted an average visual extinction in the Galactic disc of $A_G \approx 1$ mag kpc^{-1} . The extinction value varies strongly with direction and the local extinction law: in the solar neighbourhood $A_V \approx 1$ mag kpc^{-1} and $0.80 \leq A_G/A_V \leq 0.89$ for $2 \leq R_V \leq 4$ (Gontcharov et al. 2023). The average extinction of open clusters in the Galactic disc is $A_V = 0.70$ mag kpc^{-1} (Froebrich et al. 2010), but the extinction could be as low as $A_V = 0.37$ mag kpc^{-1} in diffuse regions (Wang et al. 2017) or higher in specific directions, e.g. $A_V = 1.45$ mag kpc^{-1} for open cluster King 7 (Straižys et al. 2021). We adopted an upper magnitude limit of $G = 18$ mag, as fainter stars are unlikely to have reliable parallaxes. From the absolute magnitude equation $G = M_G + 5 \log d - 5 + A_G$, where d is distance in parsecs, we find that a B3 star has an apparent G -band magnitude of 9.8 mag at 1000 pc, 14.2 mag at 3000 pc, and 15.8 mag at 4000 pc. At the cooler end of our hot star selection, an A2 main-sequence star with $T_{\text{eff}} = 8\,800$ K and absolute magnitude $M_G = 1.35$ mag would appear at G -band magnitudes of 12.3 mag at 1000 pc, 16.7 mag at 3000 pc, and 18.4 mag at 4000 pc. Because the hotter end of the temperature range contains fewer stars, this method is generally able to detect stellar populations out to distances of 3000–4000 pc.

3.2. Example

As an illustrative example, we applied this method to the YHG 6 Cas. A previous study by Maíz Apellániz et al. (2021a) identified three nearby stars with reliable *Gaia* DR2 astrometry and

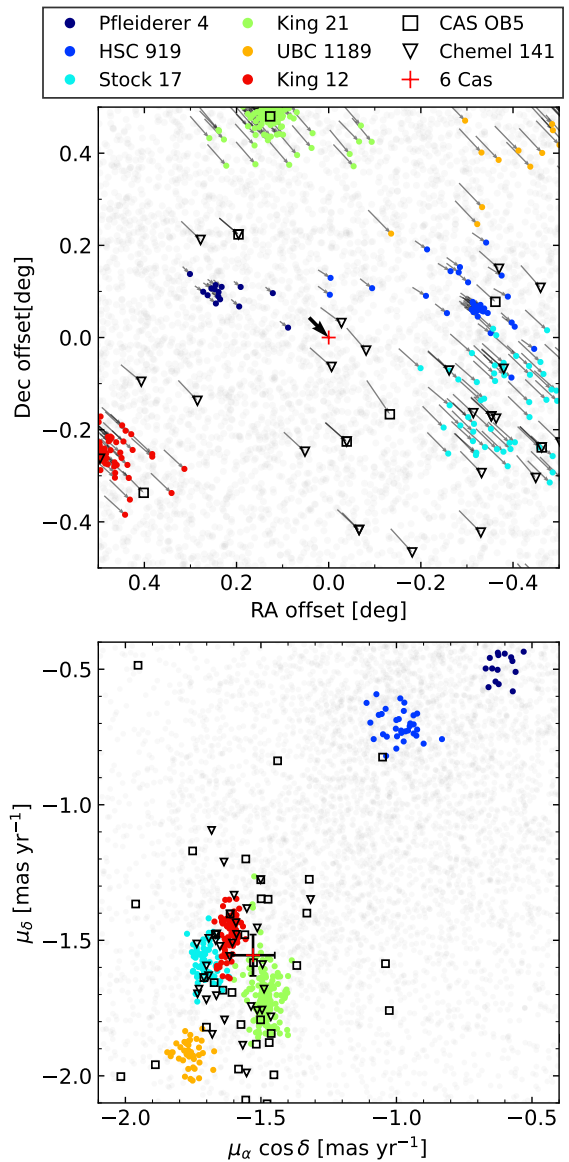


Fig. 1: Sky region around 6 Cas (red cross). Top panel: projected offsets on sky. Bottom panel: proper motions. Field stars from *Gaia* are marked in grey (one in ten has been plotted), open clusters from Hunt & Reffert (2024) are marked in coloured points, members of the OB associations Cas OB5 from Mel’nik & Dambis (2017) and no. 141 (Chemel et al. 2022) are marked with open symbols (some members overlap between the two catalogues). Arrows in the top panel indicate the motion of cluster and OB association stars over the past 0.1 Myr based on their proper motions.

derived a distance of 2780_{-290}^{+370} pc by combining their parallaxes. Figure 1 shows the sky region surrounding 6 Cas, including the positions and proper motions of nearby stars, clusters, and OB associations. 6 Cas has similar proper motion with three clusters, and OB associations Cas OB5 (Mel’nik & Dambis 2017) and no. 141 (Chemel et al. 2022).

We selected stars from *Gaia* DR3 within a $10'$ on-sky radius of 6 Cas, following the criteria listed above. The temperature criterion is informative. Figure 2 shows the distances from (Bailer-Jones et al. 2021) plotted against *Gaia* effective temperatures for hot stars within $10'$ of 6 Cas. Stars with lower tem-

¹ Using the Python code provided at https://gitlab.com/icc-ub/public/gaiadr3_zeropoint

² Using the interactive Jupyter Notebook based tool <https://github.com/ElisaHaas25/Interactive-Distance-Estimation>

³ http://www.pas.rochester.edu/~emamajek/EEM_dwarf_UBVVIJHK_colors_Teff.txt

peratures have a large scatter in distance, while stars hotter than 10 000 K seem to form a plateau just below 3000 pc.

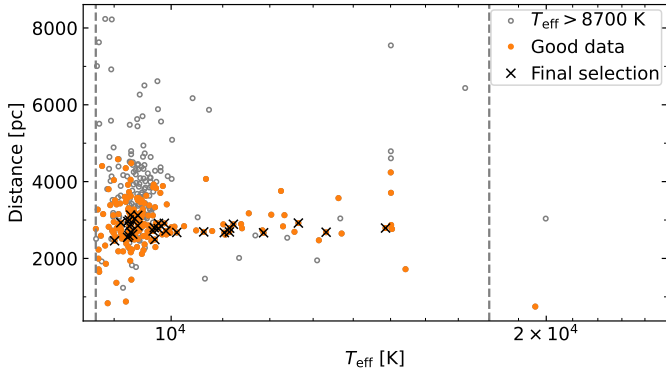


Fig. 2: *Gaia* effective temperatures and Bailer-Jones et al. (2021) distances for hot stars within 10' of 6 Cas. Stars meeting our astrometric quality criteria are highlighted in orange. The final selection of stars used for the distance estimation is marked with black crosses.

After correcting for the proper motion bias, we selected stars with proper motions similar to 6 Cas, i.e., stars with proper motions within 0.2 mas yr⁻¹ of its value (see Fig. 3). Applying the proper motion cut results in 38 stars.

We discarded any obvious outliers and stars whose parallaxes deviate by more than 2σ ($\gtrsim 0.1$ mas) from the sample mean value, resulting in a final selection of 31 stars. These stars are marked with black crosses in Fig. 2 and Fig. 3. Their consistent distances suggest that they belong to a common, association-like environment. A YSG/YHG that is no longer associated with its birth environment would not show such a tight distance grouping.

We corrected the parallaxes of the final sample for the *Gaia* zero point offset (Lindegren et al. 2021b). These offsets are small (~ 0.02 – 0.04 mas). We combined the parallaxes following the recipe of Maíz Apellániz et al. (2021b). The resulting mean parallax for 6 Cas is $\varpi = 0.3586 \pm 0.0088$. We derived a geometric distance for 6 Cas of 2790^{+70}_{-71} pc, where the errors correspond to

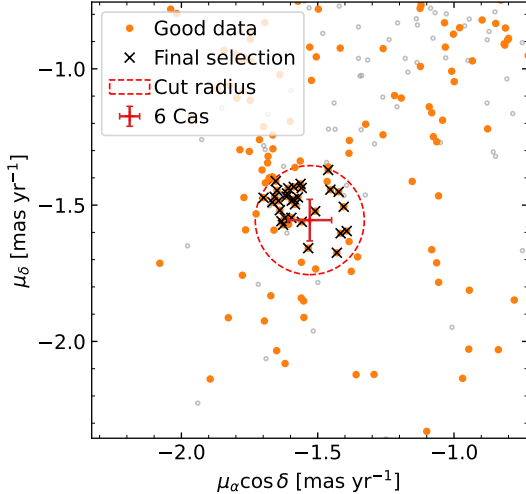


Fig. 3: Selection of stars near 6 Cas (red cross) based on proper motion, using the same sample as in Fig. 2. The proper motion cut with a radius of 0.2 mas yr⁻¹ is marked with a red circle.

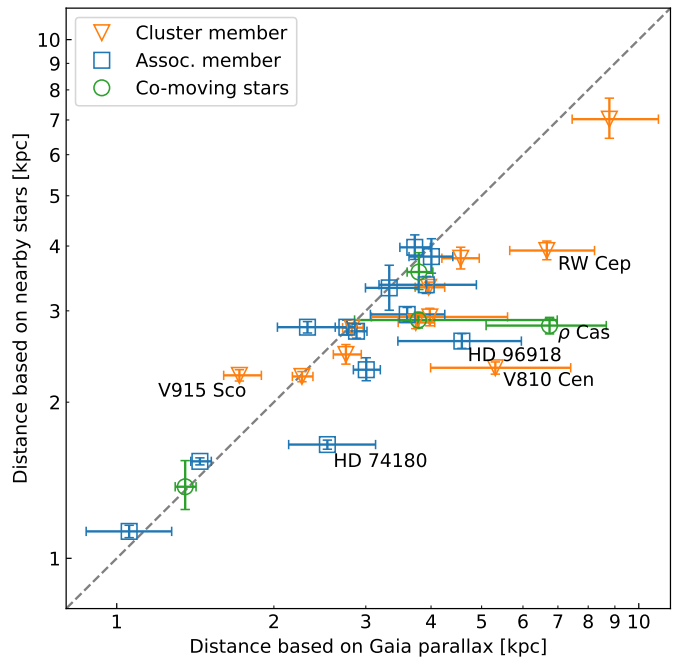


Fig. 4: Comparison of group-based distances derived in this work with distances derived from *Gaia* parallaxes by Bailer-Jones et al. (2021). Stars associated with clusters, OB association, and stars without an origin group are marked with different symbols and colours. The grey dashed line marks the one-to-one relation. Outliers are marked. Both axes are logarithmic.

the 68% confidence interval. This result agrees well with the previous estimate of 2780^{+370}_{-290} pc by Maíz Apellániz et al. (2021a).

Given the similarity in proper motion and spatial proximity to Cas OB 5, located at a distance of 2500–3000 pc (Quintana et al. 2025), we support the conclusion of Mel'nik & Dambis (2017) that 6 Cas is likely a member of this association. For the same reasons, 6 Cas may belong to association no. 141 identified by Chemel et al. (2022) at a distance of 2827 pc. The proper motion, on-sky location, and distance of Cas OB5 members identified by Mel'nik & Dambis (2017) largely overlap with stars in association no. 141 from Chemel et al. (2022), suggesting that they are the same stellar group (see Fig. 1).

3.3. Results

The group-based distances derived in this work are listed in Table 1. The proper motion cuts are illustrated in App. B and the stars used for combining the parallaxes are listed in App. C with a full table available electronically.

Figure 4 compares our group-based distances for the YHG/YSG sample with those listed in the Bailer-Jones et al. (2021) catalogue. We used the R_{GEO} values from that catalogue, as the R_{GEO} distances that consider the photometric colour indices are unlikely to reliably characterise Supergiants. For stars with relatively small parallax errors, our results agree well with the Bailer-Jones et al. (2021) catalogue values. We found significant differences for stars that have very large parallax errors, where the Bailer-Jones et al. (2021) distances tend to be very large, above 4000 pc. We found that they are likely much closer, because we identified possible affiliations with clusters or OB associations at distances 2000–3000 pc.

Overall, we improved the distance estimates for 28 stars out of the 35 stars in our sample. Of these 28 stars, 11 are cluster members, 13 are in OB associations, and four stars do not belong to a stellar group, but we found a co-moving population. For the remaining seven stars, we were unable to determine a group-based distance. IRAS 17163-3907, HD 179821, IRC +10420, V870 Sco, and IRAS 14394-6059 have co-moving stars spanning distances from 1000 pc to 4000 pc, but no clearly identifiable origin group. Most of these stars are also too distant or too reddened for this method. The final two stars, [FMR2006] 15 and IRAS 18357-0604, belong to a distant (\sim 6000 pc) stellar population rich in RSGs. We were unable to obtain group-based distances for them because of their large distance and high extinction.

4. Kinematic distances from the Galactic H₁ map

To independently verify the group-based distances derived in Sect. 3, we compared the stellar radial velocities of our targets with the kinematics of H₁ gas in the Milky Way. The H₁ gas traces both the small-scale and large-scale structures in the Galaxy (McClure-Griffiths et al. 2023, and references therein). If a star is affiliated with a cluster or an OB association, which are generally moving together with the Galactic rotation and the surrounding interstellar medium (e.g. Castro-Ginard et al. 2021), its group-based distance should be consistent with the distance inferred from the kinematics of the surrounding H₁ gas. The radial velocities of Supergiants and stars younger than 10^8 yr are correlated with the H₁ gas velocity (Fletcher 1963; Humphreys 1970).

4.1. Method

We used the spatially coherent 3D kinematic map of the H₁ gas in the Milky Way by Söding et al. (2025), based on 21-cm emission measurements from the HI4PI survey (Bekhti et al. 2016). The map is in Hierarchical Equal Area isoLatitude Pixelation of a sphere (HEALPix) format. It includes eight posterior samples for each point in the Sun-centred HEALPix-times-distance grid. We used the auxiliary fields data product by Söding et al. (2024), which includes the three components of the Galactic velocity field in each grid point. The velocity field is heliocentric, with the peculiar motion of the Sun corrected for. The bin size increases from \sim 30 pc at 2000 pc distance to \sim 100 pc at 5000 pc distance.

For each star in our sample, we extracted the line-of-sight radial velocity of the H₁ gas within a \sim 0.5 deg radius and plotted its value as a function of distance. We compared these gas velocity profiles with the stellar systemic radial velocity to determine the distance where both values are equal. We used systemic radial velocities from monitoring studies or mean radial velocities and variability amplitudes from *Gaia* DR3, where the former were not available. The adopted stellar radial velocities are listed in Table D.1. The radial-velocity variability of YHGs makes it difficult to determine accurate systemic velocities, and the gas velocity map provides accuracy at scales of hundreds of parsecs (Söding et al. 2025). Therefore, the resulting distances have uncertainties of the order of \sim 500 pc.

4.2. Examples

The gas velocity profiles and v_{rad} for six well-known YHGs are shown in Fig. 5. Depending on the shape of the H₁ velocity curve in the line-of-sight towards each star, we obtained either a sin-

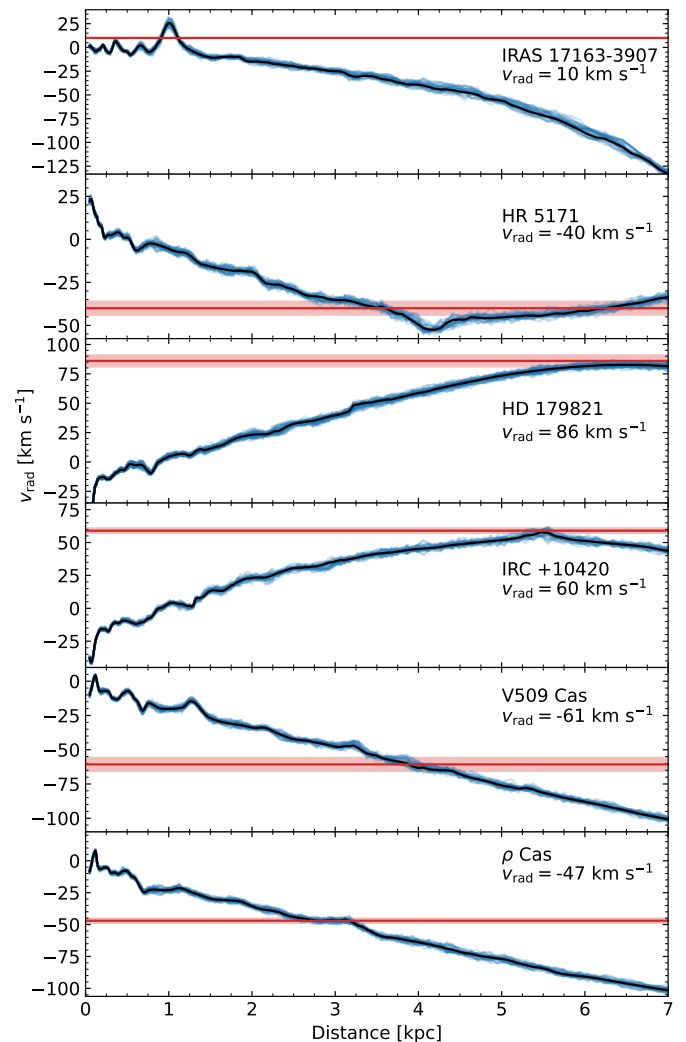


Fig. 5: Radial velocity of H₁ gas along the lines of sight towards six YHGs. The thin blue lines show the sampled posterior velocity distribution of H₁ at each distance bin within a 0.5 deg region around each star. The solid black line indicates the mean velocity. Red horizontal lines mark the observed stellar radial velocity, with the shaded region showing the approximate variability amplitude.

gle distance estimate when the stellar systemic velocity equals the gas velocity at a specific distance (e.g., V509 Cas), or a distance range when the shape of the H₁ velocity curve is flat over a distance span (e.g., ρ Cas). We highlight a few YHGs that are located in different Galactic lines-of-sights.

IRAS 17163-3907. The radial velocity of IRAS 17163-3907 with respect to the Local Standard of Rest (LSR) is 18 km s⁻¹ (Wallström et al. 2015). Transformation to the heliocentric reference frame results in a radial velocity of 9.7 km s⁻¹, which is compatible with the H₁ gas velocity near 1000 pc. We were unable to constrain a group-based distance. The H₁-based distance agrees well with the 1200^{+400}_{-200} pc distance estimate from the *Gaia* DR2 parallax (Koumpia et al. 2020) and from spectrophotometric analysis (Wallström et al. 2015). It differs significantly from the 3600–4700 pc range proposed by Lagadec et al. (2011), and from the distance derived from the *Gaia* DR3 parallax (5196^{+1401}_{-1032} pc; Bailer-Jones et al. 2021). Our result supports a shorter distance of \sim 1000 pc for IRAS 17163-3907.

HR 5171. The radial velocity of HR 5171 has been extensively monitored, with mean values of -40 km s^{-1} (Humphreys et al. 1971) and -38 km s^{-1} with a variability amplitude of 3.5 km s^{-1} (Balona 1982). This velocity corresponds to H α gas at a distance of 3500 pc, similar to the group-based distance of 2953^{+92}_{-96} pc within errors. The H α -based distance is also consistent with the established distance of 3600 pc (Humphreys et al. 1971; Chesneau et al. 2014) and with the distance from the *Gaia* parallax of 3601^{+649}_{-539} pc (Bailer-Jones et al. 2021), and does not support the 1500 ± 500 pc distance suggested by van Genderen et al. (2019). For HR 5171, a more distant distance solution at ~ 6000 pc is also possible. Such a distance ambiguity is possible for objects located in the inner Galaxy inside the solar orbit (Nakanishi & Sofue 2003). In these cases, the alternative solution is generally very small (< 1000 pc) or very large (> 5000 pc) and unlikely for most targets. We do not list them in Table 1. Our results confirm the distance of HR 5171 at 2900–3500 pc.

HD 179821. The high radial velocity of HD 179821 at 86 km s^{-1} (Şahin et al. 2016) shows good alignment with the gas velocity only at large distances (> 5000 pc), providing a lower distance limit. We were unable to constrain a group-based distance. Literature values vary from 1000 pc (Josselin & Lèbre 2001) to 6000 pc (van Genderen et al. 2019). The *Gaia* DR3 parallax is reliable, with an error of $\sim 10\%$ and a RUWE value of 0.92, corresponding to a distance of 4432^{+349}_{-355} pc (Bailer-Jones et al. 2021), which is in acceptable agreement with our result. We adopted the *Gaia* distance for this star.

IRC +10420. The radial velocity measured from emission lines in IRC+10420 is between 60 and 68 km s^{-1} (Klochkova et al. 1997; Humphreys et al. 2002), consistent with the result of CO rotational lines of $v_{\text{LSR}} 75 \text{ km s}^{-1}$ (LSR correction $\sim 16 \text{ km s}^{-1}$; Oudmaijer 1998). This velocity suggests a very large distance of 5500 pc. We were unable to constrain a group-based distance. The high distance is consistent with earlier estimates of 5800 pc (Nedoluha & Bowers 1992) and 4000–6000 pc (Jones et al. 1993) derived from Galactic rotation models. Our result is ~ 1000 pc greater than the distance derived from the *Gaia* parallax (4260^{+878}_{-752} pc). We adopted the *Gaia* distance for this star.

V509 Cas. The star has a systemic velocity of -60.7 km s^{-1} (Kasikov et al. 2024), corresponding to a H α -based distance of ~ 3800 pc. This agrees with the group-based distance of 3368 ± 127 pc within the errors. This result is significantly different from 1370 ± 480 pc based on the parallax measured by the *Hipparcos* satellite and commonly used for this star (Nieuwenhuijzen et al. 2012; van Genderen et al. 2019), but in good agreement with a distance of 3917^{+969}_{-737} pc based on its *Gaia* parallax (Bailer-Jones et al. 2021). Thus, we adopted the group-based distance.

ρ Cas. The long-term radial velocity monitoring of ρ Cas gives a well-constrained systemic velocity of $-47 \pm 2 \text{ km s}^{-1}$ (Lobel et al. 2003). This matches the H α velocity at a distance between 2500 pc and 3200 pc, in good agreement with our estimated group-based distance of 2810^{+104}_{-102} pc and the 2500 ± 500 pc distance from van Genderen et al. (2019). Thus, we adopted the group-based distance.

4.3. Results and comparison with group-based distances

The H α -based distance results are listed in Table 1. We derived H α -based distances for 32 stars, six of them lack a group-based distance estimate due to high distance and extinction. For three stars systemic radial velocities were not available. One target,

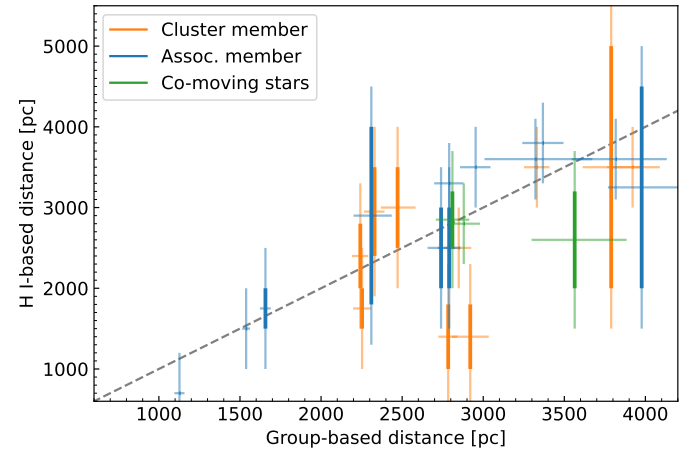


Fig. 6: Comparison of group-based and H α -based distances. Solid lines indicate the H α -based distance ranges and lighter lines illustrate the uncertainties. Affiliations with stellar groups are indicated with different colours as in Fig. 4. The grey dashed line marks the one-to-one relation.

IRAS 14394-6059, lacks both types of distance estimates, but the *Gaia* parallax places the star beyond 5000 pc, making it a potentially luminous YSG.

Six stars have only H α -based distances. Three of them, IRC+10420, HD 179821, and IRAS 17163-3907, were included in the examples above. The other three stars are [FMR2006] 15, IRAS 18357-0604, and V870 Sco. In general, the H α -based distances agree with the distances derived from the Galactic rotation. Information for all stars is included in App. A.

Generally, the results of H α -based distances coincide well with the group-based distances within the uncertainties of about 500 pc (see Fig. 6). For the group-based distances the uncertainties are of the order of 100 pc for most stars. Group-based distances are most reliable when a proper motion alignment with a cluster or OB association can be established. Otherwise, there remains a higher probability that stars with similar proper motions do not represent the birth environment. Coincidental proper motion alignment between a YSG/YHG and an unrelated OB association or open cluster at a different distance is possible. This problem becomes more severe toward the Galactic centre, where multiple stellar populations lie along the same line of sight, complicating the identification of a possible origin population and preventing reliable distance determination for several stars. Differences between the H α -based and group-based distances can indicate an incorrect origin group association or help identify potential runaway stars. Of the 26 stars that have both distance estimates, 23 stars have good agreement between the results. For three stars (ϕ Cas, HD 10494, HD 96918), we find significant discrepancies detailed below.

ϕ Cas and HD 10494. The two stars have similar radial velocities and are within 5 deg distance from each other on the sky, which corresponds to a physical separation of 270 pc using their group-based distances. The group-based distances of both stars are close to 2800 pc and are based on alignment with young clusters. For HD 10494, the group-based distance is also in good agreement with the distance derived from the *Gaia* DR3 parallax, while the parallax of ϕ Cas is unreliable. The radial velocities of ϕ Cas (-28 km s^{-1}) and HD 10494 (around -30 km s^{-1}) are very similar to their home clusters NGC 457 and NGC 654 with $v_{\text{rad}} \approx -34 \text{ km s}^{-1}$ (Rastorguev et al. 1999).

The radial velocities differ from the H₁ velocity at 2800 pc by 15–20 km s^{−1} and correspond to H₁-based distances in the range of 1000–1800 pc. This discrepancy between H₁-based and group-based distances could be a local phenomenon. These clusters are located in the Perseus arm of the Milky Way, in a region with many other young clusters. They are potential members of the Cassiopeia–Perseus open cluster complex, sharing a common origin in the same giant molecular cloud (de la Fuente Marcos & de la Fuente Marcos 2009). If this is the case, the shocks from supernovae from the previous generation of stars could have affected the kinematics of stellar populations in the region.

HD 96918. Comparison of its radial velocity with the H₁ velocity map implies a distance of ∼500 pc or of ∼5000 pc. The field around HD 96918 contains many stellar groups spanning from 500 pc to 4000 pc and aligning it with the kinematically closest OB association results in a distance of 2600 pc. Achmad et al. (1992) found the same distance ambiguity: Galactic rotation curve (500 pc or 5300 pc), interstellar reddening in line of sight (2400±900 pc), and comparing derived atmospheric parameters to evolutionary models (2200 pc). Our group-based distance result is in agreement with the latter two of their estimates. However, this discrepancy raises the possibility that the star is a runaway, which we discuss further in Section 6.2.

In the following sections, we used group-based distances when available. Otherwise, if *Gaia* $\varpi/\sigma_\varpi > 5$, we adopted the distances from Bailer-Jones et al. (2021). When neither of these are reliable, we used the H₁-based distance.

5. Radius and luminosity

Based on our distance estimates, we determined the radii and luminosities for 15 YSGs and five YHGs in our sample. In this analysis, we only included stars with available homogeneous angular diameter measurements and adopted literature T_{eff} values.

For stars with multiple published T_{eff} values, we adopted an average temperature, and for stars without spectroscopic temperature estimates, we adopted the temperature closest to their spectral type classification. Due to the inhomogeneous data and discrepancies resulting from different methods, we estimated typical temperature uncertainties of at least 200 K. For stars with multiple published T_{eff} measurements, we adopted uncertainties to encompass the range of published values. The effective temperatures of YHGs can be highly variable. In their quiescent state, they exhibit quasi-periodic pulsations with cycles of a few hundred days, with T_{eff} variability of the order of a couple hundred degrees (e.g. Kasikov et al. 2024; van Genderen et al. 2025). Temperature changes of 1000–3000 K have been observed during outbursts and on longer timescales (Lobel et al. 2003; de Jager & Nieuwenhuijzen 1997; Klochkova et al. 1997). Several YHGs, such as ρ Cas, V509 Cas, and IRC +10420, have been photometrically stable for the past decade or more and their temperatures have been determined during these quiescent phases (van Genderen et al. 2025; Nieuwenhuijzen et al. 2012; Koumpia et al. 2022). For the comparatively “normal” YSGs, the effective temperatures can differ by several hundred degrees, depending on the methods used.

5.1. Radius

To estimate the stellar radii, we used the limb-darkened angular diameter values from the JMMC Stellar Diameter Catalog (JSDC; Chelli et al. 2016; Bourgès et al. 2014; Bourges et al.

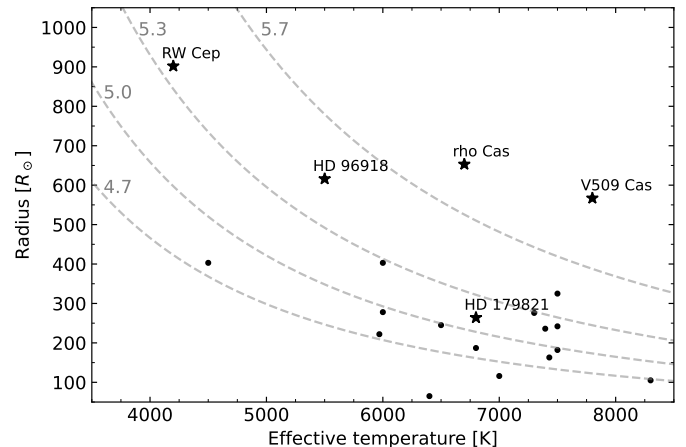


Fig. 7: Stellar radii versus T_{eff} . The YHGs are labelled, dashed grey lines indicate constant-luminosity tracks at the indicated $\log L/L_{\odot}$ values (50 000, 100 000, 200 000, and 500 000 L_{\odot} .)

2017). Out of the 35 stars in our sample, 20 are included in the JSDC catalogue, providing a homogeneous set of angular diameters based on optical and near-infrared colour indices. Of these, 19 have group-based distance values. HD 179821 does not have a group-based distance, but has a relatively good *Gaia* parallax and distance from Bailer-Jones et al. (2021). Using these distances, we calculated the stellar radii ($R/R_{\odot} = 0.1075 \theta d$, where θ is the angular diameter in milliarcseconds and d is the distance in parsecs). The results are listed in Table 2.

Fig. 7 shows the derived radii as a function of effective temperature T_{eff} with lines of constant luminosity based on the Stefan-Boltzmann law, $L \propto R^2 T_{\text{eff}}^4$. The radii of YSGs in our sample range from $100 R_{\odot}$ to $400 R_{\odot}$ with uncertainties around 10%. The radius increases with decreasing effective temperature for stars with similar luminosity. However, the most luminous YHGs – V509 Cas and ρ Cas – appear to have exceptionally large radii of ∼ $600 R_{\odot}$. To understand this result, we compared the JSDC angular diameter values with angular diameters derived from interferometric measurements.

For V509 Cas, the JSDC lists an angular diameter of 1.57 ± 0.12 mas, while the diameter measured by van Belle et al. (2009) is around 20% smaller, 1.24 ± 0.03 mas. The calculated radii are $567 \pm 111 R_{\odot}$ and $449 \pm 20 R_{\odot}$, respectively. The latter value is similar to ∼ $400 R_{\odot}$ found by Nieuwenhuijzen et al. (2012). For ρ Cas, the JSDC angular diameter is 2.16 ± 0.19 mas, while Anugu et al. (2024) determined an angular limb-darkened diameter of 2.09 ± 0.02 mas from near-infrared interferometry. Using our group-based distance, the resulting radii are $633 \pm 62 R_{\odot}$ and $609 \pm 27 R_{\odot}$, respectively. van Genderen et al. (2025) determined the radius of ρ Cas from its pulsational cycle, and found a quiescent radius of ∼ $400 R_{\odot}$ and an outburst radius of $> 700 R_{\odot}$ at a distance of 2500 pc (∼ $450 R_{\odot}$ and ∼ $780 R_{\odot}$ at our group-based distance of 2800 pc). Since the last outburst in 2013, ρ Cas has been quiescent (van Genderen et al. 2025). There is a considerable discrepancy between the radii derived from interferometric and pulsational studies.

The heterogeneous interferometric studies available for a small number of YSGs and YHGs do not allow us to consistently quantify any systematic offset between the JSDC-inferred angular diameters and those obtained from interferometric measurements. However, comparison with literature values obtained through different methods suggests that the JSDC angular diam-

Table 2: Literature data and derived radii and luminosities for the sample stars. Literature values are listed in columns labelled "Lit." together with their respective references.

Identifier	Lit. ang. diam. (mas)	Ref.	Lit. T_{eff} (K)	Ref.	Lit. radius (R_{\odot})	Lit. luminosity ($\log L/L_{\odot}$)	Ref.	Radius (R_{\odot})	Luminosity ($\log L/L_{\odot}$)
ϕ Cas	0.88 \pm 0.09	1	7200 \pm 100	2	263 \pm 34	5.23	2	276 \pm 29	5.25 $^{+0.11}_{-0.13}$
			7300 \pm 300	3	245 \pm 45	-	3		
			7341 \pm 40	4					
HD 10494	0.63 \pm 0.05	1	6672 \pm 40	4				187 \pm 15	4.83 $^{+0.09}_{-0.12}$
			7127	5					
ϵ Aur	1.95 \pm 0.20	1	7395 \pm 70	6	300	5.37	6	236 \pm 25	5.13 $^{+0.09}_{-0.12}$
HD 57118	0.55 \pm 0.05	1	7427 \pm 50	7				163 \pm 15	4.86 $^{+0.09}_{-0.10}$
R Pup	0.68 \pm 0.06	1	4100 \pm 68	8				245 \pm 22	4.98 $^{+0.09}_{-0.1}$
			6500	9					
HD 74180	1.82 \pm 0.15	1	7240	10	-	5.46	11	325 \pm 28	5.5 $^{+0.09}_{-0.11}$
			7839	5					
HD 75276	0.70 \pm 0.05	1	7100	5				116 \pm 9	4.38 $^{+0.07}_{-0.09}$
			6920 \pm 40	8					
HD 96918	2.18 \pm 0.23	1	5625 \pm 312	12	485 ^(a)	5.33 \pm 0.03	12	616 \pm 69	5.5 $^{+0.13}_{-0.2}$
			5200 \pm 200	13	700 \pm 250	5.5 \pm 0.4	13		
			5729	5	-	5.58	11		
			5866 \pm 47	8					
σ^1 Cen	1.30 \pm 0.12	1	F7 Ia	14				403 \pm 41	5.33 $^{+0.15}_{-0.21}$
			F8 Ia0	15					
V810 Cen	0.89 \pm 0.07	1	5970 \pm 100	16	420	5.3	16	222 \pm 20	4.74 $^{+0.09}_{-0.11}$
HD 144812	0.44 \pm 0.01	1	6400 \pm 100	17				65 \pm 8	3.81 $^{+0.10}_{-0.15}$
V925 Sco	0.97 \pm 0.09	1	7500	18				242 \pm 25	5.22 $^{+0.09}_{-0.12}$
HD 179821	0.56 \pm 0.01	1	7350 \pm 200	19	350 ^(b)	5.5	19	264 \pm 22	5.13 $^{+0.12}_{-0.18}$
			4900-6760	20	400-450	5.1-5.2	23		
			5900-6800	21	700 \pm 260	5.49 $^{+0.13}_{-0.19}$	24		
			6750	22	-	5.26 $^{+0.06}_{-0.08}$	25		
					-	5.47	26		
					-	5.5 \pm 0.4	22		
V1452 Aql	0.69 \pm 0.06	1	7032 \pm 50	7				182 \pm 18	4.98 $^{+0.11}_{-0.15}$
			8035	5					
V1027 Cyg	0.94 \pm 0.07	1	3930 \pm 170	27	423	4.60	27	403 \pm 37	4.78 $^{+0.17}_{-0.29}$
			5000	28					
HD 331777	0.68 \pm 0.04	1	F8Ia	29				278 \pm 23	4.96 $^{+0.08}_{-0.11}$
RW Cep	2.14 \pm 0.17	1	4200	30	900-1760	-	30	902 \pm 82	5.36 $^{+0.10}_{-0.13}$
	2.44 \pm 0.02	30			-	5.74	11		
V509 Cas	1.57 \pm 0.12	1	7500-8000	32	400-800	5.2-5.6	32	567 \pm 111 (JDSC)	6.03 $^{+0.15}_{-0.23}$ (JDSC)
	1.24 \pm 0.03	31	7800 \pm 200	33	340	-	35	449 \pm 20 (interf.)	5.83 $^{+0.05}_{-0.06}$ (interf.)
			7900 \pm 200	34	-	5.58-5.7	11		
					-	5.43	26		
HD 223767	0.35 \pm 0.01	1	A5	36				108 \pm 4	4.7 $^{+0.05}_{-0.06}$
ρ Cas	2.16 \pm 0.19	1	6000-7500	20	350-450	5.42 \pm 0.3	20	653 \pm 63 (JDSC)	5.86 $^{+0.13}_{-0.19}$ (JDSC)
	2.09 \pm 0.02	37	7300 \pm 200	34	564-700	-	37	628 \pm 24 (interf.)	5.83 $^{+0.12}_{-0.16}$ (interf.)
					450	-	35		
					-	5.66	11		
					-	5.11	26		

References. (1) Bourges et al. (2017); (2) Rosenzweig & Anderson (1993); (3) Arellano Ferro et al. (1988); (4) Kovtyukh et al. (2008); (5) Luck (2014); (6) Strassmeier et al. (2014); (7) Kovtyukh et al. (2012); (8) Usenko et al. (2011); (9) Arellano Ferro & Mantegazza (1996); (10) Forbes & Short (1994); (11) Humphreys (1978); (12) (Groenewegen 2020); (13) Achmad et al. (1992); (14) Bersier (1996); (15) Mantegazza (1992); (16) Kienzle et al. (1998); (17) Kourniotis et al. (2025); (18) Kipper (2008); (19) Şahin et al. (2016); (20) van Genderen et al. (2025); (21) Ikonnikova et al. (2018); (22) Reddy & Hrivnak (1999); (23) van Genderen et al. (2019); (24) Hawkins et al. (1995); (25) Oudmaijer et al. (2022); (26) Klochkova (2019); (27) Healy et al. (2024); (28) Klochkova et al. (2000); (29) Hackwell & Gehrz (1974); (30) Anugu et al. (2023); (31) van Belle et al. (2009); (32) Nieuwenhuijzen et al. (2012); (33) Kasikov et al. (2024); (34) Israelian et al. (1999); (35) Stothers (2012); (36) Boulon (1963); (37) Anugu et al. (2024).

Notes. For V509 Cas and ρ Cas we give the radius and luminosity values for both angular diameters: (JDSC) using the angular diameter from Bourges et al. (2017) and (interf.) using diameters from interferometric studies of van Belle et al. (2009) and Anugu et al. (2024) respectively.

^(a) Groenewegen (2020) $\log L/L_{\odot}$ = 5.33 and T_{eff} = 5625 K, using Stefan-Boltzmann law. ^(b) Şahin et al. (2016) $\log L/L_{\odot}$ = 5.5 and T_{eff} = 7350 K, using Stefan-Boltzmann law.

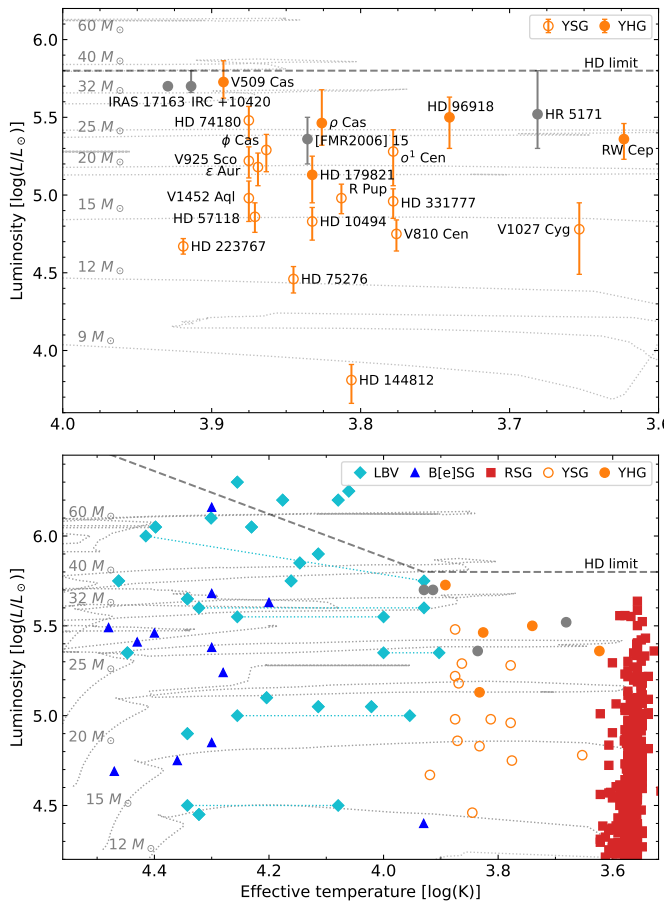


Fig. 8: YHGs and YSGs on the HR diagram. YHGs are shown as filled yellow circles, YSGs and candidate YHGs as empty yellow circles. Literature values for four YHGs are shown as grey circles. The HD luminosity limit (Humphreys 1978) is marked with a dashed line. Solar-metallicity evolutionary tracks (Ekström et al. 2012) are shown as light grey dotted lines. Top panel: YHGs and YSGs only. Bottom panel: For comparison, literature data for Galactic RSGs (red squares; Healy et al. 2024), LBVs (cyan diamonds; Smith et al. 2019), and B[e] Supergiant stars (blue triangles; Miroshnichenko et al. 2025) are shown.

eters for V509 Cas and ρ Cas are likely overestimated. The JSDC empirical relations between angular diameters and photometric indices for luminosity classes I, II and III are primarily calibrated on K- and M-type giants, with very few hotter stars included (Chelli et al. 2016). For luminous Supergiants in advanced evolutionary states, these relations may not apply. In addition, the colours of YHGs are intrinsically variable (van Genderen et al. 2019), which may contribute to the uncertainty in determining diameters from photometric indices. With limited and heterogeneous interferometric measurements available, we cannot establish systematic offsets between angular diameters from the JSDC and those obtained from interferometric measurements. Homogeneously derived angular diameters from the spectral energy distribution or interferometric modelling are required to obtain self-consistent radii for the sample stars.

5.2. Luminosity

Using the stellar radii derived for 20 stars in the previous section, we estimated the stellar luminosities using the Stefan-

Boltzmann law. The resulting luminosities are listed in Table 2, together with literature values for comparison. For studies reporting bolometric magnitudes, we converted them to luminosity using $\log L/L_\odot = 0.4(-M_{\text{bol}} + 4.74)$ (Mamajek et al. 2015).

The luminosities of YSGs and YHGs are shown in the top panel of Fig. 8. For V509 Cas and ρ Cas, we used the radii from Nieuwenhuijzen et al. (2012) and van Genderen et al. (2025) instead of the JSDC values due to the concern of overestimated angular diameters. IRC +10420, IRAS 17163-3907, [FMR2006] 15, and HR 5171 do not have angular diameters listed in the JSDC, but we adopted their luminosities from the literature for reference. The bottom panel of Fig. 8 shows the high-luminosity region of the HR diagram, including the B[e] Supergiants (B[e]SGs), Luminous Blue Variables (LBVs), and RSGs. The LBV and B[e]SG luminosities have significant error bars, which are not displayed for clarity.

In the HR diagram, most YHGs occupy the region above $\log L/L_\odot > 5.4$, which corresponds to $M_{\text{ini}} = 25 - 40 M_\odot$. Three stars lie near the Humphreys-Davidson (HD) luminosity limit: IRC +10420, IRAS 17163-3907, and V509 Cas. The YSGs occupy a wider range of luminosities, with the most luminous YSGs partially overlapping with the less luminous YHGs. The luminosities of three YHGs, HD 179821, RW Cep, and HD 96918, are in good agreement with previous studies. Significant deviations are found for V509 Cas and ρ Cas, where using the angular diameters from JSDC results in unexpectedly large radii and unreasonably high luminosities ($\log L/L_\odot > 5.8$). Although for ρ Cas, the large radius is supported by an interferometric study (Anugu et al. 2024). The calculated luminosities for YSGs are generally in very good agreement with literature values. We only find a discrepancy for V810 Cen, where the previous luminosity estimate of $\log L/L_\odot = 5.3$ (Kienzle et al. 1998) is much higher than our value of $\log L/L_\odot = 4.74^{+0.09}_{-0.11}$ due to a revised, lower distance by ~ 1000 pc.

6. Discussion

6.1. Spatial distribution

Following discussions on the spatial distribution and possible isolation of LBVs and Supergiants with the B[e] phenomenon (e.g. Smith & Tombleson 2015; Aadland et al. 2018; Deman & Oey 2024; Martin et al. 2025, and references therein), van Genderen et al. (2019) proposed that the YHGs ρ Cas, V509 Cas, HR 5171, and HD 179821 are isolated objects, which could be evidence of an evolutionary connection with LBVs. An explanation for the potential isolation of LBVs is their origin through binary evolution – either as merger product or as mass gainer in Roche-lobe overflow systems that were kicked out of their original population after their companion exploded as a stripped-envelope supernova Smith & Tombleson (2015).

Fig. 9 shows the locations of our sample stars projected on a schematic view of the Milky Way. We used the group-based distances where available, otherwise the H₁-based or Bailer-Jones et al. (2021) distances. The stars broadly trace the spiral arms of the Galaxy. Our results indicate that YHGs are located in heterogeneous environments. Two YHGs are likely cluster members, three are in OB associations, and one is in a star forming region. Four YHGs may be unaffiliated to stellar groups, but two of them are too far to draw a clear conclusion.

In contrast, a majority of the YSGs in our sample are associated with stellar groups. 20 out of 25 YSGs have kinematic

⁴ NASA/JPL-Caltech/R. Hurt (SSC/Caltech)

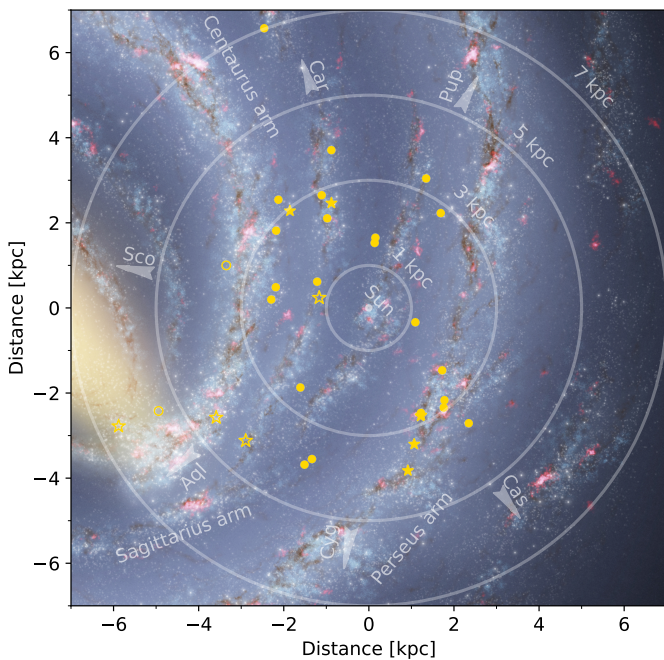


Fig. 9: A family portrait. Illustration of the Milky Way⁴ showing the distribution of YSGs (circles) and YHGs (stars). Objects with group-based distances are marked with filled markers and objects with distances based on H₁ or Bailer-Jones et al. (2021) are marked with empty markers.

properties consistent with membership in open clusters or OB associations. For five stars, no clear origin group could be found. In two of these cases, V870 Sco and IRAS 14394-6059, the stars are distant and have high extinction. For the other three stars, HD 12399, α^1 Cen, and HD 144812, we can identify co-moving stars sharing a similar distance.

Overall, we found that most YSGs are members of young stellar populations. This is consistent with YSGs being younger, pre-RSG objects and still affiliated to their birth environments. The environments of the YHGs are more diverse, and for almost half of them their origin populations remain unclear. This could be the result of different evolutionary histories. If so, there may be multiple ways for a star to become a YHG, and the distance from their birth environments may be a result of binary interactions.

The number of luminous YSGs found in the Large Magellanic Cloud (Martin & Humphreys 2023) is more than double the size of our sample and could provide more insight into their surrounding environments. Improved astrometry and distances of Galactic YSGs and YHGs will be provided by the *Gaia* DR4 release⁵, which will include epoch astrometry for all sources.

6.2. Runaway stars

Around 25–30% of Galactic O-type stars are runaway stars, and about a quarter of these show bow shocks generated from the interaction between their stellar winds and the interstellar medium (Carretero-Castrillo et al. 2023, 2025). Studies in the SMC suggest that around 65% of OB-type field stars are runaways, mainly due to dynamical ejections from clusters (Dorigo Jones et al. 2020, and references therein). Since OB stars are the progenitors

of YHGs/YSGs, some stars in our sample may have experienced an ejection event. The YHGs in our sample without clear group affiliation have variable stellar winds and have undergone major mass-loss events (e.g. Lobel et al. 2003; Oudmaijer 1998; Koumpia et al. 2020; Jura & Werner 1999), setting ideal conditions for bow shock formation in a runaway scenario. However, we found no evidence of a bow shock associated with any YHG or YSG in our sample, either in the literature or in our examination of Wide-Field Infrared Survey Explorer (*WISE*; Wright et al. 2010) images.

For stars where the H₁-based and group-based distance estimates are in good agreement, a runaway scenario is unlikely, as dynamical perturbations would affect the proper motion, radial velocity, or both, leading to inconsistent distances. An exception is HD 96918, for which the proper motion aligns with OB associations no. 210/211 (Chemel et al. 2022), yielding a group distance of 2623^{+88}_{-83} pc, but the H₁-based distance is ~ 500 pc or ~ 5000 pc. This discrepancy was already identified by Achmad et al. (1992), whose distance estimates of 2400 ± 900 pc and ~ 2200 pc from independent methods are in good agreement with our group-based distance. If HD 96918 were a runaway, an apparent alignment with an OB association based on similar proper motion would be unlikely to provide a reliable distance. If HD 96918 has been dynamically perturbed, its radial velocity could deviate from the H₁ velocity, but the effect has not been significant enough to separate it from the stars in the OB association.

Small offsets in proper motions ($> 2\sigma$ of the cluster's mean) are observed for several cluster members: ϕ Cas, HD 18391, and RW Cep have minor proper motion offsets compared to other members of their clusters (Appendix B). HD 223767 has a projected on-sky offset of < 0.1 deg of the open cluster King 12 and shares a similar distance of ~ 2800 pc, but its proper motion differs from cluster members by more than 3σ . HD 74180 lies near the open clusters Pismis 6 and Pismis 8, both at distances of ~ 1700 pc and separated by ~ 0.3 deg on sky, with proper motion differences of ~ 0.5 mas yr⁻¹. These cluster may originate from the same molecular cloud (Fitzgerald et al. 1979). A proper motion difference of 0.5 mas yr⁻¹ corresponds to a velocity difference of ~ 5 km s⁻¹ at a distance of 2000 pc and ~ 7 km s⁻¹ at 3000 pc, indicating small kinematical differences originating from modest dynamical interactions. Overall, while we found minor kinematic offsets for several stars, we found no clear evidence of runaway YHGs or YSGs in our sample.

6.3. Comments on binarity

The binary fraction for YSGs is not well constrained. Recently, a multiplicity study in the Small Magellanic Cloud (SMC) suggested that Supergiants of spectral classes B, A, and F were born as effectively single stars or are products of binary mergers (Patrick et al. 2025). For AF-type Supergiants in the SMC, the binary fraction was estimated to be less than 15% (Patrick et al. 2025). However, O'Grady et al. (2024) estimated the binary fraction of YSGs in the Magellanic Clouds at 20–60%. For reference, O-type stars in the Milky Way have a binary fraction of ~ 70 –90% (Sana et al. 2012, 2014), and the observed binary fraction for RSGs in the SMC and Large Magellanic Cloud (LMC) is ~ 15 –30% (Neugent et al. 2020; Dorda & Patrick 2021; Patrick et al. 2019, 2020; Dai et al. 2025).

We reprise that a majority of the well-studied YHGs are likely to have binary companions: HR 5171 is a double or triple system, where one companion could be interacting with the

⁵ <https://www.cosmos.esa.int/web/gaia/dr4>

Hypergiant (Chesneau et al. 2014). 6 Cas is an A+O-type Superiant binary (Maíz Apellániz et al. 2021a). V509 Cas has a likely B-type companion (Lobel et al. 2013). IRAS 17163-3907 has been suggested to have a binary companion (Wallström et al. 2017). ρ Cas, IRC +10420, and [FMR2006] 15 have RUWE values higher than 1.22, which is the threshold commonly used as an indicator for unresolved binarity (Castro-Ginard et al. 2024). Only HD 179821 appears to be single, as it is unlikely to have a companion more massive than $5 M_{\odot}$ and a spectral class earlier than B5 (Jura & Werner 1999).

Among the YSGs, less information is available, but some confirmed cases of binarity include: ϵ Aur is an eclipsing binary (Stefanik et al. 2010); HD 144812 is an interacting binary (Kourniotis et al. 2025); V915 Sco has a Wolf-Rayet companion (Andrews 1977); V810 Cen is a spectroscopic binary (Kienzle et al. 1998); ϕ Cas and HD 57118 have been identified as binaries (Burki & Mayor 1983); and HD 96918, HD 74180, and IRAS 18357-0604 have high RUWE values.

Overall, about 50% of the YHGs and YSGs in our sample show direct or indirect signs of binarity, with a firm lower limit of 22% (eight confirmed binary systems). We selected our sample based on luminosity estimates in the literature and did not consider any binarity indicators. Nevertheless, these factors are correlated through the contribution of a hot companion to the overall luminosity of the system, which may introduce a bias towards identifying binaries.

7. Conclusions

In this study, we provided a homogeneous and consistent determination of distances for Galactic YSGs and YHGs. Due to the uncertainties in the *Gaia* parallaxes, we explored an indirect method of distance determination through membership identification with nearby stellar groups – clusters or OB associations. We compared the proper motions of YHGs and YSGs with those of clusters (Hunt & Reffert 2024) and OB associations (Chemel et al. 2022; Mel’nik & Dambis 2017) in the surrounding sky region. Using the more reliable parallaxes of co-moving stars, we calculated “group-based” distances. We validated this method against the large-scale Galactic kinematics by comparing the stellar systemic radial velocities with the Galactic H α velocity map (Söding et al. 2025). Our “H α -based” distances agree well with previous studies, where distances were derived from comparison with the Galactic rotation curve. The two independent methods show good agreement for majority of the targets.

We determined membership in a cluster or OB association for 20 YSGs. Five YSGs remain without a clearly identified stellar group, two of them are likely too distant and reddened for the method. The stellar environments of YHGs are more varied:

- Stellar cluster: RW Cep, [FMR2006] 15
- OB association: 6 Cas, V509 Cas, HD 96918
- Star forming region: HR 5171
- Unaffiliated: ρ Cas, IRAS 17163-3907, IRC +10420, HD 179821

We derived luminosities for 15 YSGs and 5 YHGs by combining our distance estimates with T_{eff} values from the literature and angular diameters from the JSDC catalogue. Our results are generally in good agreement with previous luminosity estimates. The upcoming *Gaia* DR4 will improve the astrometric measurements and allow for further studies of stellar environments surrounding YHGs and YSGs. A homogeneous interferometric survey of Galactic YSGs and YHGs would be valuable to better

constrain the radii and luminosities, determine the binary fraction, and study the circumstellar environments. Future work will address the circumstellar environments and spectral energy distributions of YSGs and YHGs.

Acknowledgements. We would like to thank Willem-Jan de Wit, Evgenia Koumpia, and Rain Kipper for insightful discussions. This work has made use of data from the European Space Agency (ESA) mission *Gaia* (<https://www.cosmos.esa.int/gaia>), processed by the *Gaia* Data Processing and Analysis Consortium (DPAC, <https://www.cosmos.esa.int/web/gaia/dpac/consortium>). Funding for the DPAC has been provided by national institutions, in particular the institutions participating in the *Gaia* Multilateral Agreement. This research has made use of the Jean-Marie Mariotti Center JSDC catalogue, which involves the JMDC catalogue. JSDC available at <http://www.jmmc.fr/jcdc>. Part of this work was supported by the Estonian Research Council grant PRG 2159. This research has made use of the VizieR catalogue access tool, CDS, Strasbourg, France.

References

Aadland, E., Massey, P., Neugent, K. F., & Drout, M. R. 2018, AJ, 156, 294
 Achmad, L., Lamers, H. J. G. L. M., Nieuwenhuijzen, H., & van Genderen, A. M. 1992, A&A, 259, 600
 Aidelman, Y., Cidale, L. S., Zorec, J., & Panei, J. A. 2015, A&A, 577, A45
 Aldering, G., Humphreys, R. M., & Richmond, M. 1994, AJ, 107, 662
 Anderson, L. D., Bania, T. M., Balsler, D. S., et al. 2014, ApJS, 212, 1
 Andrews, J. P. 1977, MNRAS, 178, 131
 Anugu, N., Baron, F., Gies, D. R., et al. 2023, AJ, 166, 78
 Anugu, N., Baron, F., Monnier, J. D., et al. 2024, ApJ, 974, 113
 Arellano Ferro, A. & Mantegazza, L. 1996, A&A, 315, 542
 Arellano Ferro, A. & Parrao, L. 1990, A&A, 239, 205
 Arellano Ferro, A., Parrao, L., & Giridhar, S. 1988, PASP, 100, 993
 Arnal, E. M., Duronea, N. U., & Testori, J. C. 2008, A&A, 486, 807
 Bailer-Jones, C. A. L., Rybizki, J., Fouesneau, M., Demleitner, M., & Andrae, R. 2021, AJ, 161, 147
 Balona, L. A. 1982, MNRAS, 201, 105
 Bekhti, N. B., Flöer, L., Keller, R., et al. 2016, A&A, 594, A116
 Bersier, D. 1996, A&A, 308, 514
 Boulon, J. 1963, Journal des Observateurs, 46, 243
 Bourges, L., Mella, G., Lafrasse, S., et al. 2017, VizieR Online Data Catalog, 2346, II/346
 Bourges, L., Lafrasse, S., Mella, G., et al. 2014, in ASP conference series, ed. N. Manset & P. Forshay, Vol. 485, 223
 Burki, G. & Mayor, M. 1983, A&A, 124, 256
 Campillay, A. R., Arias, J. I., Barbá, R. H., et al. 2019, MNRAS, 484, 2137
 Cantat-Gaudin, T. & Brandt, T. D. 2021, A&A, 649, A124
 Carretero-Castrillo, M., Benaglia, P., Paredes, J. M., & Ribó, M. 2025, A&A, 694, A250
 Carretero-Castrillo, M., Ribó, M., & Paredes, J. M. 2023, A&A, 679, A109
 Castro-Ginard, A., McMillan, P. J., Luri, X., et al. 2021, A&A, 652, A162
 Castro-Ginard, A., Penoyre, Z., Casey, A. R., et al. 2024, A&A, 688, A1
 Chelli, A., Duvert, G., Bourgès, L., et al. 2016, A&A, 589, A112
 Chemel, A. A., de Grij, R., Glushkova, E. V., & Dambis, A. K. 2022, MNRAS, 515, 4359
 Chesneau, O., Meilland, A., Chapellier, E., et al. 2014, A&A, 563, A71
 Chiavassa, A., Pasquato, E., Jorissen, A., et al. 2011, A&A, 528, A120
 Clark, J. S., Negueruela, I., & González-Fernández, C. 2014, A&A, 561, A15
 Crockett, R. M., Eldridge, J. J., Smartt, S. J., et al. 2008, MNRAS, 391, L5
 Dai, M., Wang, S., & Jiang, B. 2025, MNRAS, 539, 1220
 Damiani, F., Micela, G., & Sciortino, S. 2016, A&A, 596, A82
 Davies, B., Figer, D. F., Kudritzki, R.-P., et al. 2007, ApJ, 671, 781
 Davies, B., Figer, D. F., Law, C. J., et al. 2008, ApJ, 676, 1016
 de Jager, C. 1998, A&AR, 8, 145
 de Jager, C. & Nieuwenhuijzen, H. 1997, MNRAS, 290, L50
 de la Fuente Marcos, R. & de la Fuente Marcos, C. 2009, New Astronomy, 14, 180
 De Medeiros, J. R., Udry, S., Burki, G., & Mayor, M. 2002, A&A, 395, 97
 Delgado, A. J., Djupvik, A. A., Costado, M. T., & Alfaro, E. J. 2013, MNRAS, 435, 429
 Deman, J. A. & Oey, M. S. 2024, ApJ, 976, 125
 Dorda, R. & Patrick, L. R. 2021, MNRAS, 502, 4890
 Dorigo Jones, J., Oey, M. S., Paggeot, K., Castro, N., & Moe, M. 2020, ApJ, 903, 43
 Dorn-Wallenstein, T. Z., Neugent, K. F., & Levesque, E. M. 2023, ApJ, 959, 102
 Ekström, S., Georgy, C., Eggenberger, P., et al. 2012, A&A, 537, A146
 El-Badry, K. 2025, The Open Journal of Astrophysics, 8, 62

El-Badry, K., Lam, C., Holl, B., et al. 2024, The Open Journal of Astrophysics, 7, 100

Fabricius, C., Luri, X., Arenou, F., et al. 2021, A&A, 649, A5

Figer, D. F., MacKenty, J. W., Robberto, M., et al. 2006, ApJ, 643, 1166

Fitton, S., Tofflemire, B. M., & Kraus, A. L. 2022, Res. Notes AAS, 6, 18

Fitzgerald, M. P., Boudreault, R., Fich, M., Luiken, M., & Witt, A. N. 1979, A&AS, 37, 351

Fletcher, E. S. 1963, AJ, 68, 407

Forbes, D. & Short, S. 1994, AJ, 108, 594

Froebrich, D., Schmeja, S., Samuel, D., & Lucas, P. W. 2010, MNRAS, 409, 1281

Gaia Collaboration, Montegriffo, P., Bellazzini, M., et al. 2023, A&A, 674, A33

Gaia Collaboration, Prusti, T., de Bruijne, J. H. J., et al. 2016, A&A, 595, A1

Gontcharov, G. A. 2006, Astronomy Letters, 32, 759

Gontcharov, G. A., Marchuk, A. A., Khovrachev, M. Y., et al. 2023, Astronomy Letters, 49, 673

Groenewegen, M. A. T. 2020, A&A, 635, A33

Guinan, E. F., Mayer, P., Harmanec, P., et al. 2012, A&A, 546, A123

Hackwell, J. A. & Gehrz, R. D. 1974, ApJ, 194, 49

Hawkins, G. W., Skinner, C. J., Meixner, M. M., et al. 1995, ApJ, 452, 314

He, Z., Liu, X., Luo, Y., Wang, K., & Jiang, Q. 2023a, ApJS, 264, 8

He, Z., Luo, Y., Wang, K., et al. 2023b, ApJS, 267, 34

Healy, S., Horiuchi, S., Colomer Molla, M., et al. 2024, MNRAS, 529, 3630

Herbig, G. H. 1972, ApJ, 174, L89

Holl, B., Sozzetti, A., Sahlmann, J., et al. 2023, A&A, 674, A10

Humphreys, R. M. 1970, AJ, 75, 602

Humphreys, R. M. 1978, ApJS, 38, 309

Humphreys, R. M., Davidson, K., & Smith, N. 2002, AJ, 124, 1026

Humphreys, R. M., Jones, T. J., & Martin, J. C. 2023, AJ, 166, 50

Humphreys, R. M., Strecker, D. W., & Ney, E. P. 1971, ApJ, 167, L35

Hunt, E. L. & Reffert, S. 2024, A&A, 686, A42

Ikonomikova, N. P., Taranova, O. G., Arkhipova, V. P., et al. 2018, Astronomy Letters, 44, 457

Israelian, G., Lobel, A., & Schmidt, M. R. 1999, ApJ, 523, L145

Jones, T. J., Humphreys, R. M., Gehrz, R. D., et al. 1993, ApJ, 411, 323

Josselin, E. & Lèbre, A. 2001, A&A, 367, 826

Jura, M. & Werner, M. W. 1999, ApJ, 525, 113

Karr, J. L., Manoj, P., & Ohashi, N. 2009, ApJ, 697, 133

Kasikov, A., Kolka, I., Aret, A., et al. 2025, A&A, 694, A153

Kasikov, A., Kolka, I., Aret, A., Eennäe, T., & Checha, V. 2024, A&A, 686, A270

Kienzle, F., Burki, G., Burnet, M., & Meynet, G. 1998, A&A, 337, 779

Kilpatrick, C. D., Foley, R. J., Abramson, L. E., et al. 2017, MNRAS, 465, 4650

Kipper, T. 2008, Baltic Astronomy, 17, 311

Klochkova, V. G. 2019, Astrophysical Bulletin, 74, 475

Klochkova, V. G., Chentsov, E. L., & Panchuk, V. E. 1997, MNRAS, 292, 19

Klochkova, V. G., Mischenina, T. V., & Panchuk, V. E. 2000, Astronomy Letters, 26, 398

Klochkova, V. G., Panchuk, V. E., & Tavolanskaya, N. S. 2016, Astronomy Letters, 42, 815

Koumpia, E., Oudmaijer, R. D., de Wit, W.-J., et al. 2022, MNRAS, 515, 2766

Koumpia, E., Oudmaijer, R. D., Graham, V., et al. 2020, A&A, 635, A183

Kourniotis, M., Kraus, M., Arias, M. L., & Cidale, L. S. 2025, MNRAS, 540, L28

Kovtyukh, V. V., Chekhonadskikh, F. A., Luck, R. E., et al. 2010, MNRAS, 408, 1568

Kovtyukh, V. V., Gorlova, N. I., & Belik, S. I. 2012, MNRAS, 423, 3268

Kovtyukh, V. V., Soubiran, C., Luck, R. E., et al. 2008, MNRAS, 389, 1336

Lagadec, E., Zijlstra, A. A., Oudmaijer, R. D., et al. 2011, A&A, 534, L10

Lindegren, L., Bastian, U., Biermann, M., et al. 2021a, A&A, 649, A4

Lindegren, L., Klioner, S. A., Hernández, J., et al. 2021b, A&A, 649, A2

Lobel, A., de Jager, K., & Nieuwenhuijzen, H. 2013, in ASP Conference Series, ed. G. Pugliese, A. de Koter, & M. Wijburg, Vol. 470, 167

Lobel, A., Dupree, A. K., Stefanik, R. P., et al. 2003, ApJ, 583, 923

Luck, R. E. 2014, AJ, 147, 137

Maas, T. 2003, Ph.D. thesis

Mamajek, E. E., Torres, G., Prsa, A., et al. 2015, in IAU 2015 Resolution B2

Mantegazza, L. 1992, A&A, 265, 527

Maravelias, G., Bonanos, A. Z., Antoniadis, K., et al. 2025, ArXiv e-prints [arXiv:2504.01232]

Marco, A., Negueruela, I., Castro, N., & Simón-Díaz, S. 2025, MNRAS, 542, 703

Martin, J. C. & Humphreys, R. M. 2023, AJ, 166, 214

Martin, J. C., Humphreys, R. M., & Davidson, K. 2025, ArXiv e-prints [arXiv:2508.17114]

Maund, J. R., Fraser, M., Ergon, M., et al. 2011, ApJ, 739, L37

Maíz Apellániz, J., Barbá, R. H., Fariña, C., et al. 2021a, A&A, 646, A11

Maíz Apellániz, J. & Negueruela, I. 2025, in Proceedings of the XVI Scientific Meeting of the Spanish Astronomical Society, ed. M. Manteiga, F. G. Galindo, A. L. Ortega, M. M. González, N. Rea, M. R. Gómez, A. U. Miguel, G. Yepes, C. R. López, A. G. García, & C. Dafonte, 224

Maíz Apellániz, J., Pantaleoni González, M., & Barbá, R. H. 2021b, A&A, 649, A13

McClure-Griffiths, N. M., Stanimirović, S., & Rybicky, D. R. 2023, ARA&A, 61, 19

Mel'nik, A. M. & Dambis, A. K. 2017, MNRAS, 472, 3887

Melnik, A. M. & Dambis, A. K. 2020, MNRAS, 493, 2339

Miroshnichenko, A. S., Zharikov, S. V., Vaidman, N. L., & Khokhlov, S. A. 2025, in Proceedings of the IAU Symposium 402, ed. A. Wofford, N. St-Louis, M. García, & S. Simón-Díaz (Cambridge University Press)

Moffat, A. F. J., Fitzgerald, M. P., & Jackson, P. D. 1977, ApJ, 215, 106

Nakanishi, H. & Sofue, Y. 2003, PASJ, 55, 191

Nedoluha, G. E. & Bowers, P. F. 1992, ApJ, 392, 249

Negueruela, I., Alfaro, E. J., Dorda, R., et al. 2022, A&A, 664, A146

Neugent, K. F., Levesque, E. M., Massey, P., Morrell, N. I., & Drout, M. R. 2020, ApJ, 900, 118

Nieuwenhuijzen, H., De Jager, C., Kolka, I., et al. 2012, A&A, 546, A105

Niu, Z., Sun, N.-C., & Liu, J. 2024, ApJ, 970, L9

O'Grady, A. J. G., Drout, M. R., Neugent, K. F., et al. 2024, ApJ, 975, 29

Oksala, M. E., Kraus, M., Cidale, L. S., Muratore, M. F., & Borges Fernandes, M. 2013, A&A, 558, A17

Oudmaijer, R. D. 1998, A&AS, 129, 541

Oudmaijer, R. D., Groenewegen, M. A. T., Matthews, H. E., Blommaert, J. A. D. L., & Sahu, K. C. 1996, MNRAS, 280, 1062

Oudmaijer, R. D., Jones, E. R. M., & Vioque, M. 2022, MNRAS, 516, L61

Parsons, S. B. 1981, ApJ, 245, 201

Pasquato, E., Pourbaix, D., & Jorissen, A. 2011, A&A, 532, A13

Patrick, L. R., Lennon, D. J., Britavskiy, N., et al. 2019, A&A, 624, A129

Patrick, L. R., Lennon, D. J., Evans, C. J., et al. 2020, A&A, 635, A29

Patrick, L. R., Lennon, D. J., Najarro, F., et al. 2025, A&A, 698, A39

Perren, G., Vázquez, R., & Carraro, G. 2012, A&A, 548, A125

Quintana, A. L., Negueruela, I., & Berlanas, S. R. 2025, A&A, 697, A47

Rastorguev, A. S., Glushkova, E. V., Dambis, A. K., & Zabolotskikh, M. V. 1999, Astronomy Letters, 25, 595

Reddy, B. E. & Hrivnak, B. J. 1999, AJ, 117, 1834

Reed, B. C. 2000, AJ, 119, 1855

Reguitti, A., Pastorello, A., Smartt, S. J., et al. 2025, A&A, 698, A129

Robinson, G., Thomas, J. A., Hirst, R. A., & Hyland, A. R. 1973, PASP, 85, 436

Rosenzweig, P. & Anderson, L. 1993, ApJ, 411, 207

Sana, H., de Mink, S. E., de Koter, A., et al. 2012, Science, 337, 444

Sana, H., Le Bouquin, J.-B., Lacour, S., et al. 2014, ApJS, 215, 15

Smith, N., Aghakhanloo, M., Murphy, J. W., et al. 2019, MNRAS, 488, 1760

Smith, N. & Tombleson, R. 2015, MNRAS, 447, 598

Smolinski, J., Climenhaga, J. L., & Harris, B. L. 1980, Acta Astron., 30, 427

Stefanik, R. P., Torres, G., Lovegrove, J., et al. 2010, AJ, 139, 1254

Stothers, R. B. 2012, ApJ, 751, 151

Straižys, V., Kazlauskas, A., Boyle, R. P., et al. 2021, AJ, 162, 224

Strassmeier, K. G., Weber, M., Granzier, T., et al. 2014, Astron. Nachr., 335, 904

Söding, L., Edenhofer, G., Enßlin, T., et al. 2024, Zenodo [zenodo:12578443]

Söding, L., Edenhofer, G., Enßlin, T. A., et al. 2025, A&A, 693, A139

Tartaglia, L., Fraser, M., Sand, D. J., et al. 2017, ApJ, 836, L12

Turner, D. G. 1982, PASP, 94, 655

Turner, D. G., Kovtyukh, V. V., Majaess, D. J., Lane, D. J., & Moncrieff, K. E. 2009, Astron. Nachr., 330, 807

Usenko, I. A., Kniazev, A. Y., Berdnikov, L. N., & Kravtsov, V. V. 2011, Astronomy Letters, 37, 499

van Belle, G. T., Creech-Eakman, M. J., & Hart, A. 2009, MNRAS, 394, 1925

van Genderen, A. M., Lobel, A., Nieuwenhuijzen, H., et al. 2019, A&A, 631, A48

van Genderen, A. M., Lobel, A., Timmerman, R., et al. 2025, A&A, 694, A136

Vasquez, J., Cappa, C., & McClure-Griffiths, N. M. 2005, MNRAS, 362, 681

Wallström, S. H. J., Lagadec, E., Muller, S., et al. 2017, A&A, 597, A99

Wallström, S. H. J., Muller, S., Lagadec, E., et al. 2015, A&A, 574, A139

Wang, S., Jiang, B. W., Zhao, H., Chen, X., & de Grijs, R. 2017, ApJ, 848, 106

Wegner, W. 2006, MNRAS, 371, 185

White, S. D. M. 1975, ApJ, 197, 67

Wright, E. L., Eisenhardt, P. R. M., Mainzer, A. K., et al. 2010, AJ, 140, 1868

Wu, Y. W., Xu, Y., Menten, K. M., Zheng, X. W., & Reid, M. J. 2012, in Proceedings of the IAU Symposium, ed. R. Booth, E. Humphreys, & W. Vlemmings, Vol. 287, 425–426

Zsoldos, E. & Percy, J. R. 1991, A&A, 246, 441

Şahin, T., Lambert, D. L., Klochkova, V. G., & Panchuk, V. E. 2016, MNRAS, 461, 4071

Appendix A: Notes on individual targets

In this section, we provide a brief overview of the analysis performed for the individual targets. Unless stated otherwise, the parameters used to select nearby stars are the same as those described in Sect. 3.

ϕ Cas. The *Gaia* DR3 parallax is low-quality ($\varpi/\sigma_\varpi = 2.6$). Its on-sky location coincides with the cluster NGC 457 (2800 ± 9 pc; Hunt & Reffert 2024) and it has been included as a cluster member (Arellano Ferro & Parrao 1990; Rastorguev et al. 1999). Its proper motion does not support cluster membership, but the errors are relatively large (~ 0.06 mas yr^{-1}). We applied a 0.4 mas yr^{-1} proper motion cut around ϕ Cas' value on stars within $10'$ of the target. We calculated a group distance of 2920^{+114}_{-113} pc, consistent with membership in cluster NGC 457. The radial velocity of ϕ Cas from *Gaia* DR3 is -19.2 ± 3 km s^{-1} , while other studies report values near -28 km s^{-1} (Arellano Ferro et al. 1988; Rosenzweig & Anderson 1993). The last is similar to the cluster radial velocity of -34 km s^{-1} (Rastorguev et al. 1999). Using the radial velocity -28 km s^{-1} , we found a H α -based distance in the range of 1000–1800 pc, much closer than the cluster. Both the star's and the cluster's radial velocities are inconsistent with the H α radial velocity at 2800 pc. We found the cluster NGC 457 to be the most likely origin population.

HD 10494. The *Gaia* DR3 parallax is high-quality ($\varpi/\sigma_\varpi = 19.8$), resulting in a distance of 2823^{+142}_{-114} pc (Bailer-Jones et al. 2021). The on-sky location of HD 10494 coincides with the cluster NGC 654 (2815 ± 11 pc; Hunt & Reffert 2024) and the star has been included as a cluster member (Arellano Ferro & Parrao 1990; Rastorguev et al. 1999) and a member of the OB association Cas OB8 in the same sky region (Mel'nik & Dambis 2017). Its proper motion is in good agreement (2σ) with cluster membership. The proper motion also aligns very well with the OB association no. 150 at a distance of 2626 pc (Chemel et al. 2022). We applied a 0.2 mas yr^{-1} proper motion cut around HD 10494's value on stars within $10'$ of the target. We calculated a group distance of 2784^{+57}_{-61} pc, very similar to the Bailer-Jones et al. (2021) distance. The radial velocity from *Gaia* DR3, -30.6 km s^{-1} , agrees well with the cluster velocity of -33.8 km s^{-1} (Rastorguev et al. 1999). We found a H α -based distance in the range of 1000–1800 pc, with a similar discrepancy as for ϕ Cas. The two stars lie within 5° of each other on the sky, which corresponds to a physical distance of ~ 270 pc at their group-based distances.

HD 12399. The *Gaia* DR3 parallax is high-quality ($\varpi/\sigma_\varpi = 14.3$), resulting in a distance of 3792^{+240}_{-192} pc (Bailer-Jones et al. 2021). Its on-sky location and proper motion are not aligned with any known cluster or OB association. We applied a 0.3 mas yr^{-1} proper motion cut around HD 12399's value on stars within $10'$ of the target. Most stars within the cut have distances > 3500 pc, but their parallaxes are low quality. There are six foreground stars at 2200–2700 pc, but given the high-quality parallax of HD 12399, the farther population is more likely. Among the more distant stars, only four stars have $\varpi/\sigma_\varpi > 5$. We calculated a group distance of 3564^{+320}_{-266} pc. Using the *Gaia* DR3 radial velocity of -44 ± 8 km s^{-1} , we found a H α -based distance in the range of 2000–3200 pc.

HD 18391. The *Gaia* DR3 parallax is high-quality ($\varpi/\sigma_\varpi = 18.6$), resulting in a distance of 2263^{+113}_{-93} (Bailer-Jones et al. 2021). The on-sky location of HD 18391 coincides with the sparse open cluster SAI 25 (2252 ± 11 pc; Hunt & Reffert 2024), Turner et al. (2009) described its home cluster as 'Anonymous' and determined a shorter distance of 1661 ± 73 pc. Its proper

motion is in agreement (3σ) with membership in SAI 25. The proper motion also aligns very well with the OB association no. 143 at a distance of 2262 pc (Chemel et al. 2022). We applied a 0.3 mas yr^{-1} proper motion cut around HD 18391's value on stars within $10'$ of the target. We calculated a group distance of 2242^{+49}_{-52} pc. Using the *Gaia* DR3 radial velocity of -39 ± 3 km s^{-1} , we found a H α -based distance in the range of 2000–2800 pc.

ϵ Aur. The *Gaia* DR3 parallax is medium-quality ($\varpi/\sigma_\varpi = 5.5$) resulting in a distance of 1056^{+218}_{-182} pc (Bailer-Jones et al. 2021). It has a high RUWE value of 1.71 and large proper motion uncertainties (~ 0.2 mas yr^{-1}). Its on-sky location and proper motion are not aligned with any known cluster. It has been identified as a member of the Aur OB1 association (Arellano Ferro & Parrao 1990; Mel'nik & Dambis 2017). On-sky, it is close to OB association no. 147 at a distance of 1154 pc (Chemel et al. 2022), though its proper motion differs by ~ 0.6 mas yr^{-1} from the association members. But given the large errors, we consider the proper motions similar enough. Within $20'$ of the target we found most stars at distances > 2000 pc. There are very few hot stars at ~ 1000 pc and they are scattered in proper motions. We applied a very wide 1.6 mas yr^{-1} proper motion cut around ϵ Aur's value and found only four stars. The group-based distance is 1127 ± 31 pc. Using the radial velocity of -2.3 km s^{-1} (Stefanik et al. 2010), we found a H α -based distance of ~ 700 pc, consistent with the closer group distance.

HD 57118. The *Gaia* DR3 parallax is high-quality ($\varpi/\sigma_\varpi = 18$), resulting in a distance of 2759^{+116}_{-138} pc. It is a member of the OB association no. 25 at a distance of 2524 pc (Chemel et al. 2022). We applied a 1 mas yr^{-1} proper motion cut around HD 57118's value on stars within $10'$ of the target. We calculated a group distance of 2790^{+88}_{-93} pc. Using the *Gaia* DR3 radial velocity 61.2 ± 1.4 km s^{-1} , we found a H α -based distance of ~ 3300 pc.

R Pup. The *Gaia* DR3 parallax is high-quality ($\varpi/\sigma_\varpi = 13.5$), resulting in a distance of 3958^{+291}_{-228} pc. The on-sky location of R Pup coincides with the cluster NGC 2439 (3350 ± 13 pc; Hunt & Reffert 2024) of which it is a member (Arellano Ferro & Parrao 1990; White 1975). Its proper motion is in good agreement (1σ) with cluster membership. The proper motion also aligns very well with the OB association no. 68 at a distance of 3237 pc (Chemel et al. 2022). We applied a 0.1 mas yr^{-1} proper motion cut around R Pup's value on stars within $10'$ of the target. We calculated a group distance of 3331^{+77}_{-80} pc. Using the radial velocity of 62.5 km s^{-1} (Balona 1982), we found a H α -based distance of ~ 4000 pc.

HD 74180. The *Gaia* DR3 parallax is medium-quality ($\varpi/\sigma_\varpi = 4.3$), resulting in a distance of 2532^{+600}_{-397} pc. It has high RUWE value of 2.56 and large proper motion uncertainties (~ 0.1 mas yr^{-1}). It has been identified as a member of the Vel OB1 association (Mel'nik & Dambis 2017; Humphreys 1978; Reed 2000). The proper motion aligns with the OB association no. 107 at a distance of 1935 pc (Chemel et al. 2022). The star has been proposed to be affiliated with the region of the open cluster NGC 2645 (Pismis 6; Forbes & Short 1994) at a distance of 1720 ± 5 pc (Hunt & Reffert 2024), although it is not considered a member (Aidelman et al. 2015). Its proper motion has a ~ 0.5 mas yr^{-1} offset from the members of NGC 2645. The cluster radial velocity of 20.8 ± 3 km s^{-1} (Rastorguev et al. 1999) is similar to the radial velocity of HD 74180 of 25 ± 3 km s^{-1} (Forbes & Short 1994). We applied a 0.5 mas yr^{-1} proper motion cut around HD 74180's value on stars within $20'$ of the target. Hot stars with similar proper motion to HD 74180 are lo-

cated at cluster distance. Because its proper motion does not align clearly with the cluster, we do not count it as a member, but we found it to be affiliated with the same region, in agreement with Forbes & Short (1994). We calculated a group distance of 1657^{+33}_{-34} pc. Using the radial velocity of 25 km s^{-1} (Forbes & Short 1994), we found a H α -based distance in the range of 1500–2000 pc.

HD 75276. The *Gaia* DR3 parallax is high-quality ($\varpi/\sigma_\varpi = 19$), resulting in a distance of 1443^{+74}_{-57} pc. It has been identified as a member of the Vel OB1 association (Mel'nik & Dambis 2017; Reed 2000). The proper motion aligns with the OB association no. 106 at a distance of 1447 pc or no. 107 at a distance of 1935 pc (Chemel et al. 2022). In the 10' field of view, there is a low number of hot stars with similar proper motions and parallax, and there is a significant distant population at ~ 3000 pc. We applied a 0.7 mas yr^{-1} proper motion cut around HD 75276's value on stars within 10' of the target and excluded the background stars. We calculated a group distance of 1538 ± 24 pc. Using the *Gaia* DR3 radial velocity of $\sim 26 \text{ km s}^{-1}$, we found a H α -based distance of ~ 1500 pc. De Medeiros et al. (2002) suggested a slightly lower velocity of 21 km s^{-1} and Reed (2000) derived a higher velocity of $\sim 32 \text{ km s}^{-1}$. These velocities decrease or increase the distance estimate by a couple of hundred parsecs.

V709 Car. The *Gaia* DR3 parallax is high-quality ($\varpi/\sigma_\varpi = 8.1$), resulting in a distance of 4006^{+397}_{-376} . We did not find alignment with any known cluster or OB association. In the 10' field of view there is a significant population of hot stars at ~ 4000 pc with proper motions similar to V709 Car, but their parallax errors are large. We applied a 0.25 mas yr^{-1} proper motion cut around V709 Car's value, excluded likely foreground stars at ~ 2000 pc, and relaxed the parallax quality criterion to $\varpi/\sigma_\varpi = 3$. We calculated a group distance of 3817^{+315}_{-271} pc. V709 Car is a binary system with a period of 323 days, its radial velocity varies between ~ 6 – 18 km s^{-1} (Maas 2003). Using an average radial velocity of 12 km s^{-1} , we found a H α -based distance of ~ 3600 pc.

TYC 8958-479-1. The *Gaia* DR3 parallax is medium-quality ($\varpi/\sigma_\varpi = 3$), resulting in a distance of 8783^{+2122}_{-1330} pc. Maíz Apellániz & Negueruela (2025) identified the star as a member of the open cluster Barbá 2 at a distance of 7390^{+650}_{-550} . Its proper motion also aligns with the OB association no. 8 (Chemel et al. 2022) at a distance of 6917 pc. The Barbá 2 cluster is not included in the Hunt & Reffert (2024) catalogue, thus we do not include cluster membership in the identified cluster column of Table 1. We applied a 0.1 mas yr^{-1} proper motion cut around TYC 8958-479-1's value on stars within 10' of the target and identified four hot stars at this large distance with reliable parallaxes. We calculated a group distance of 7025^{+687}_{-572} pc. We are unaware of any radial velocity measurements to compare with the H α kinematics.

HD 96918. The *Gaia* DR3 parallax is low-quality ($\varpi/\sigma_\varpi = 2.2$). The star has a high RUWE value of 1.99 and large proper motion uncertainties ($\sim 0.1 \text{ mas yr}^{-1}$). It has been identified as a member of the CarOB2 association (Mel'nik & Dambis 2017; Humphreys 1978). On the sky, it is located at the edge of the open cluster NGC 3532 (distance 472 pc; Hunt & Reffert 2024), but its proper motion differs from the cluster members by $\sim 4 \text{ mas yr}^{-1}$, and thus is incompatible with membership. We found a relatively good alignment in proper motion with the OB associations 210 and 211 at distances of 2362 pc and 2450 pc (Chemel et al. 2022), but they are $\sim 1^\circ$ away on the sky. We applied a 0.4 mas yr^{-1} proper motion cut around HD 96918's value on stars within 10' of the target. We found stellar populations at ~ 2500 pc and at ~ 4000 pc. Based on previous distance estimates

in the literature – 1900 pc (Luck 2014), 2000 pc (Groenewegen 2020), and 2700 pc (Achmad et al. 1992) – HD 96918 is more likely part of the closer population. We calculated a group distance of 2623^{+88}_{-83} pc. Using the radial velocity of 5.6 km s^{-1} (Balona 1982), we found a H α -based distance of ~ 5000 pc or ~ 500 pc, similar to the result found by Achmad et al. (1992). This discrepancy is addressed in Sect. 4.3.

$\alpha^1 \text{ Cen}$. The *Gaia* DR3 parallax is medium-quality ($\varpi/\sigma_\varpi = 4.43$), resulting in a distance of 3783^{+3197}_{-928} pc. We did not find alignment with any known cluster or OB association. We applied a 0.6 mas yr^{-1} proper motion cut around $\alpha^1 \text{ Cen}$'s value on stars within 20' of the target. We found a population at ~ 3000 pc with similar proper motion to $\alpha^1 \text{ Cen}$, no foreground group, but a significant background population at > 5000 pc. We calculated a group distance of 2880 ± 100 pc. Using the radial velocity of -21 km s^{-1} (Gontcharov 2006), we found a H α -based distance of ~ 2800 pc.

V810 Cen. The *Gaia* DR3 parallax is low-quality ($\varpi/\sigma_\varpi = 1.7$). The star has large proper motion uncertainties ($\sim 0.1 \text{ mas yr}^{-1}$) likely due to binarity. It has been identified as a member of the open cluster Stock 14 (Kovtyukh et al. 2010) at a distance of 2340 ± 9 pc (Hunt & Reffert 2024) and also as a background star (Kienzle et al. 1998). On-sky, it is located within the cluster Stock 14. The Hunt & Reffert (2024) catalogue lists two other open clusters in the same sky region: Theia 2727 (3655^{+52}_{-50} pc) and Lynga 15 (1646 ± 8 pc). The proper motion does not align with any of the clusters. Within a 10' field of view, we applied a proper motion cut with a radius of 0.4 mas yr^{-1} around V810 Cen and found stellar populations at the distance of Stock 14 and a farther beyond 3000 pc. Kienzle et al. (1998) assumed, based on previous spectroscopic analysis, that the blue companion has a B0-B1 Iab-Ib spectral type and thus an absolute magnitude $M_V \simeq -6$ mag, suggesting a distance greater than 3000 pc. However, in a more recent analysis (Wegner 2006), these supergiant spectral types correspond to $-5.22 \leq M_V \leq -4.65$ mag, consistent with $M_V = -4.6$ mag found by Parsons (1981) who assumed a cluster distance of 2600 pc. Another indication of the closer distance is given by interstellar extinction. $E(B - V)$ is in the range of 0.24–0.3 for both Stock 14 and V810 Cen (Parsons 1981; Kienzle et al. 1998). Within 10' of the target we found low extinction for stars at a distance of 2200–2500 pc (monochromatic extinction from *Gaia* $0.5 \leq A_0 \leq 1$), and much higher extinction for stars at distances of 3000–4000 pc, with A_0 increasing from 2 to 4 or even 5. In Wide-Field Infrared Survey Explorer (*WISE*; Wright et al. 2010) band 3 (12 μm) and band 4 (22 μm) images, a dense structure can be seen at the location of Stock 14, which corresponds to the H α region GAL 295.14-00.63 (Anderson et al. 2014). We extracted the H α number density from the map of Söding et al. (2025) in the line-of-sight towards V810 Cen, and found that it increases beyond 2000 pc and peaks at ~ 2800 pc. This suggests that the H α region lies beyond the cluster Stock 14, causing enhanced extinction for its background stars. Due to the low reddening of V810 Cen, it cannot be located within this region and must be part of a closer population. We calculated a group distance of 2330^{+61}_{-65} pc for the closer population. We also found a nearby OB association, no. 205 at a distance of 2347 pc Chemel et al. (2022), that overlaps with the Cru OB1 association (Mel'nik & Dambis 2017). The proper motion of the stars in the OB association are a better match for V810 Cen than the Stock 14 stars, but most of its members in the Chemel et al. (2022) catalogue are more than 1 deg away on sky. Using the radial velocity of $v_{\text{rad}} = -17 \text{ km s}^{-1}$ (Kienzle et al. 1998), we found a H α -based distance in the range of 2400–3200 pc.

HR 5171. The *Gaia* DR3 parallax is medium-quality ($\varpi/\sigma_\varpi = 4.79$), resulting in a distance of 3601^{+649}_{-539} pc. The YHG HR 5171 has been associated with the star-forming region Gum 48d/R 80 (Karr et al. 2009, and references therein). Its on-sky location and proper motion are not aligned with any known cluster or OB association. We applied a 0.4 mas yr^{-1} proper motion cut around HR 5171's value on stars within $10'$ of the target. We found a relatively smooth distribution of stellar populations between 2000 and 3500 pc with two population peaks at distances 2300 pc and 2900 pc. Stars at farther distances have high parallax uncertainties, likely due to increased extinction in the H II region Gum 48d (R 80) located at a distance of 2900 pc (Melnik & Dambis 2020) or 3600 pc (Karr et al. 2009). Most stars with proper motions similar to HR 5171 belong to the 2900 pc population. We calculated a group distance of 2953^{+92}_{-96} pc, which we adopted for HR 5171, but the distance could be higher, as the hot stars with similar proper motions at farther distances are not taken into account because of high parallax uncertainties. The group-based distance of the foreground population is 2297^{+63}_{-65} pc, which could be considered a lower limit for the distance for HR 5171. HR 5171A has a companion HR 5171B, which is a B0Ib spectral type supergiant (Humphreys et al. 1971; Karr et al. 2009) with a high-quality parallax value ($\varpi/\sigma_\varpi = 19$) and a distance of 2879^{+148}_{-134} pc (Bailer-Jones et al. 2021). Using the radial velocity of $v_{\text{rad}} = 40 \text{ km s}^{-1}$ (Balona 1982; Humphreys et al. 1971), we found a H I-based distance of ~ 3500 pc (see Fig. 5). Thus, HR 5171 is at a distance of 2900–3600 pc for four reasons: 1) good agreement with H I kinematics and Galactic rotation curve; 2) stellar group at that distance; 3) agreement with the *Gaia* parallax-based distance of 3601^{+649}_{-539} ($\varpi/\sigma_\varpi \approx 5$; Bailer-Jones et al. 2021); 4) the companion has a similar distance with high-quality quality parallax.

UCAC2 4867478. The *Gaia* DR3 parallax is medium-quality ($\varpi/\sigma_\varpi = 6.2$), resulting in a distance of 3327^{+465}_{-331} pc. We did not find alignment with any known cluster or OB association. We applied a 0.2 mas yr^{-1} proper motion cut around UCAC2 4867478's value on stars within $10'$ of the target. We found a group of hot stars with very similar proper motions and parallaxes. We relaxed the parallax quality criterion to $\varpi/\sigma_\varpi = 3$ and calculated a group distance of 3322^{+351}_{-314} pc. Using the *Gaia* DR3 radial velocity of $-41 \pm 4 \text{ km s}^{-1}$, we found a H I-based distance of ~ 3600 pc.

IRAS 14394-6059. The *Gaia* DR3 parallax is medium-quality ($\varpi/\sigma_\varpi = 5.3$, resulting in a distance of 5450^{+770}_{-686} pc (Bailer-Jones et al. 2021). We did not find alignment with any known cluster or OB association. Within a $10'$ field of view, we tried different proper motion cuts and found hot stars scattered over a wide range of distances from 2000 pc to 5000 pc. The parallaxes of distant stars have very high uncertainties and we have no way to disentangle the populations. We are not aware of any radial velocity measurements to derive H I-based distance. If the *Gaia* parallax is reliable, it is potentially a luminous YSG.

CD-59 5594. The *Gaia* DR3 parallax is high-quality ($\varpi/\sigma_\varpi = 10.33$), resulting in a distance of 3739^{+325}_{-279} pc (Bailer-Jones et al. 2021). The star's proper motion aligns with the cluster Pismis 21 at a distance of 2906 ± 24 pc (Hunt & Reffert 2024) and with the OB association no. 47 at 2958 pc (Chemel et al. 2022). We applied a 0.15 mas yr^{-1} proper motion cut around CD-59 5594's value on stars within $10'$ of the target. We calculated a group distance of 2849 ± 77 pc. Using the *Gaia* DR3 radial velocity of $-36 \pm 4 \text{ km s}^{-1}$, we found a H I-based distance of ~ 2500 pc.

HD 144812. The *Gaia* DR3 parallax is high-quality ($\varpi/\sigma_\varpi = 21.55$), resulting in a distance of 1352^{+66}_{-58} pc (Bailer-Jones et al. 2021). However, the RUWE value is high (1.37). Kourniotis et al. (2025) proposed that HD 144812 has a companion of spectral class B2.5 or hotter. The proper motion of HD 144812 does not align with any known cluster or OB association. Within a $10'$ field of view, we found very few hot stars. We applied a 0.5 mas yr^{-1} proper motion cut around HD 144812's value and found only four stars with $T_{\text{eff}} > 7500$ K: two with distances ~ 1300 pc and two with distances ~ 1500 pc. The group-based distance estimate for these four stars is 1454^{+52}_{-51} pc. Increasing the cut radius did not show any farther population with similar kinematics. We are unaware of any radial velocity measurements to calculate a H I-based distance. We explored the effect of the high RUWE value on the distance uncertainty of HD 144812. El-Badry (2025) derived a function that describes the parallax uncertainty inflation factor, f , which takes the higher RUWE values into account. To calculate f , we used the analytic function given in Eq. 3 of El-Badry (2025). In addition to the RUWE value, the inflation factor depends on the parallax itself and an empirical along-scan measurement, σ_η , which is a function of G -magnitude, (see Sect. 2 in El-Badry et al. 2024, for a detailed description). HD 144812 has $G = 7.9$ mag, and based on Fig. 3 in Holl et al. (2023), we adopted $\sigma_\eta \approx 0.2$ mas. We calculated an inflation factor of $f = 2.3$, resulting in a corrected parallax uncertainty of $\sigma_\varpi = 0.0773$. For the parallax itself, we applied the zero-point correction (Lindgren et al. 2021a). The resulting corrected parallax is $\varpi = 0.7497 \pm 0.0773$ mas. Even after inflating the parallax error, $\varpi/\sigma_\varpi = 9.34$, indicating a parallax uncertainty of $\sim 10\%$ and confirming that the *Gaia* parallax of HD 144812 is reasonably reliable. Based on the corrected parallax we derived a geometric distance of 1374^{+169}_{-132} pc, which we adopt for HD 144812.

V870 Sco. The *Gaia* DR3 parallax is medium-quality ($\varpi/\sigma_\varpi = 3.87$), resulting in a distance of 3945^{+940}_{-642} pc (Bailer-Jones et al. 2021). On the sky, it is located in the open cluster NGC 6231 (distance 1553 ± 2 pc; Hunt & Reffert 2024), but V870 Sco is significantly more reddened than the cluster members ($A_V \approx 10.0$) and has been proposed as a background star (Damiani et al. 2016). This might be a result of an optically thick circumstellar shell or that the star lies behind the cluster, as its radial velocity is different from the cluster members (Robinson et al. 1973; Damiani et al. 2016). Its *Gaia* proper motion differs by 1.5 mas yr^{-1} from the cluster members. Detecting a background population is challenging due to the high extinction behind the cluster. We tested $10'$ and $20'$ fields of view, but the results remain inconclusive. Thus, we are not able to align V870 Sco with any known stellar cluster or association. Using the *Gaia* DR3 radial velocity of $-43 \pm 5 \text{ km s}^{-1}$, we found a H I-based distance of ~ 3500 pc. The radial velocity of -53 km s^{-1} from Herbig (1972) results in a distance of ~ 4000 pc, both in agreement with the Bailer-Jones et al. (2021) distance.

V915 Sco. The *Gaia* DR3 parallax is high-quality ($\varpi/\sigma_\varpi = 10.44$), resulting in a distance of 1809^{+191}_{-182} pc (Bailer-Jones et al. 2021). V915 Sco is a luminous YSG (HD 155603A) with a Wolf-Rayet WN companion WR 85 (HD 155603B; Andrews 1977). On the sky, it is located in the open cluster HSC 2870 at a distance of 2350 ± 25 pc (Hunt & Reffert 2024) and its proper motion aligns with it (1σ). The proper motion also aligns with the OB association no. 82 at a distance of 2250 pc (Chemel et al. 2022). We applied a 0.2 mas yr^{-1} proper motion cut around V915 Sco's value on stars within $10'$ of the target. We calculated a group distance of 2253^{+57}_{-56} pc. Using the radial velocity of

-6 km s^{-1} (Andrews 1977), we found a H α -based distance in the range of 1200–2000 pc.

IRAS 17163-3907. The *Gaia* DR3 parallax is low-quality ($\varpi/\sigma_\varpi = 1.95$). According to literature, IRAS 17163-3907 could be a member of the star forming region RCW 122 at a distance of 3380^{+330}_{-270} pc (Wu et al. 2012) or 5000 pc (Arnal et al. 2008). The radial velocity of the molecular cloud has been measured at $v_{\text{LSR}} = -15 \text{ km s}^{-1}$, where gas with velocity from -23 to -8 km s^{-1} is expected to be physically associated (Arnal et al. 2008). These values differ from the star's systemic velocity $v_{\text{LSR}} = 18 \text{ km s}^{-1}$ (Wallström et al. 2017). Calculations using luminosity and the star's high visual extinction suggest a 1000 pc distance (Wallström et al. 2015) and the distance derived from *Gaia* DR2 parallax, 1200^{+400}_{-200} pc, has been used by Koumpia et al. (2020). A distance between 3600 pc and 4700 pc was suggested by Lagadec et al. (2011). We found no alignment with any known stellar cluster or OB association, but note that due to the high extinction in this region, any stars farther than 3000 pc could be too faint for reliable parallaxes. Using the $v_{\text{LSR}} = 18 \text{ km s}^{-1}$ (Wallström et al. 2017) and an LSR correction of $\sim 8 \text{ km s}^{-1}$, we found a H α -based distance of ~ 1000 pc (see Fig. 5).

V925 Sco. The *Gaia* DR3 parallax is high-quality ($\varpi/\sigma_\varpi = 12.76$), resulting in a distance of 3006^{+192}_{-166} pc. It has been identified as a member of Trumpler 27 (Moffat et al. 1977), although this cluster might be a collection of stellar populations extending from 1500 to 5000 pc rather than a compact group (Perren et al. 2012). In the open cluster catalogue of Hunt & Reffert (2024), there are two clusters in roughly the same sky region at different distances: OC 697 ($\varpi = 0.397 \pm 0.045$ mas, distance 2282 ± 12 pc) and UFMG 82 ($\varpi = 0.59 \pm 0.05$ mas, distance 1550 ± 9 pc), both have Tr 27 as an alternate designation. We were unable to find reliable radial velocities for the clusters. This could offer an explanation for the uncertain distance of Tr 27 with results from different authors varying from 1000 to 2000 pc (Moffat et al. 1977). The proper motion of V925 Sco does not align with the members of either of these open clusters. It is in slightly better alignment with association no. 82, at a distance of 2250 pc Chemel et al. (2022), close to OC 697. We applied a 0.3 mas yr^{-1} proper motion cut around V925 Sco's value on stars within $10'$ of the target. We found stellar groups at two distances: at 2310^{+126}_{-110} pc, the neighbourhood of OC 697, and at 3110^{+359}_{-298} pc, a more distant population. V925 Sco could belong to either population, but due to the proper motion similarity with the OB association we list the closer distance in Table 1. Using the *Gaia* DR3 radial velocity of -15.6 km s^{-1} , we found a H α -based distance in the range of 1800 to 4000 pc. Because we are looking in the direction of the Galactic centre, the H α velocity profile is rather flat around -12 km s^{-1} over a wide distance range.

[FMR2006] 15. The *Gaia* DR3 parallax is low-quality ($\varpi/\sigma_\varpi = 1.23$). This star is a member of the Red Supergiant Cluster 1 (RSGC 1) at a large distance of 5800 pc (Figer et al. 2006) or 6600 ± 890 pc (Davies et al. 2008). It is too distant to reliably detect a stellar group of hot stars. Using the radial velocity of $v_{\text{LSR}} = 120.8 \text{ km s}^{-1}$ (Davies et al. 2008) with an LSR correction of 15 km s^{-1} , we found a H α -based distance of ~ 6500 pc.

IRAS 18357-0604. The *Gaia* DR3 parallax is negative. This star has a very similar proper motion to nearby supergiants belonging to the cluster RSGC 2, at a distance of 5830^{+1910}_{-780} pc (Davies et al. 2007). Using the radial velocity of $90 \pm 3 \text{ km s}^{-1}$ (Clark et al. 2014), we found a H α -based distance of 5500 pc.

HD 179821. The *Gaia* DR3 parallax is high-quality ($\varpi/\sigma_\varpi = 9.2$), resulting in a distance of 4432^{+349}_{-355} pc (Bailer-Jones et al. 2021). We found no alignment with any known cluster or OB association, but the star may be too distant. Using the radial velocity of $85.8 \pm 0.8 \text{ km s}^{-1}$ (Şahin et al. 2016), we found a H α -based distance of > 5000 pc.

V1452 Aql. The *Gaia* DR3 parallax is high-quality ($\varpi/\sigma_\varpi = 15.5$), resulting in a distance of 2748^{+193}_{-148} pc (Bailer-Jones et al. 2021). This star has been identified as a member of the open cluster CWN 1591 (He et al. 2023b). We applied a 0.25 mas yr^{-1} proper motion cut around V1452 Aql's value on stars within $10'$ of the target. We calculated a group distance of 2472^{+111}_{-104} pc. Using the *Gaia* DR3 radial velocity of $33 \pm 8 \text{ km s}^{-1}$, we found a H α -based distance in the range of 2500–3500 pc.

IRC +10420. The *Gaia* DR3 parallax is medium-quality ($\varpi/\sigma_\varpi = 3.43$), resulting in a distance of 4260^{+878}_{-752} pc. We did not find alignment with any known cluster or OB association, but the star may be too distant. Using the radial velocity of $\sim 60 \text{ km s}^{-1}$ (Klochkova et al. 1997; Jones et al. 1993; Oudmaijer et al. 1996), we found a H α -based distance of ~ 5500 pc. This is in agreement with previous distance estimates in the range of 4000–6000 pc (Jones et al. 1993; Reddy & Hrivnak 1999).

V1027 Cyg. The *Gaia* DR3 parallax is high-quality ($\varpi/\sigma_\varpi = 13.45$), resulting in a distance of 3723^{+265}_{-237} pc. The star's proper motion aligns with the OB association no. 15 at a distance of 3902 pc (Chemel et al. 2022). We applied a 0.1 mas yr^{-1} proper motion cut around V1027 Cyg's value on stars within $10'$ of the target. We calculated a group distance of 3977^{+226}_{-208} pc. Using the *Gaia* DR3 radial velocity of $8.7 \pm 10.3 \text{ km s}^{-1}$, we found a H α -based distance in a very wide range of 2000–4500 pc.

HD 331777. The *Gaia* DR3 parallax is high-quality ($\varpi/\sigma_\varpi = 11.58$), resulting in a distance of 4559^{+388}_{-363} pc. On the sky, the star is located within the open cluster Kronberger 54 at a distance of 4025^{+73}_{-70} pc (Hunt & Reffert 2024) and its proper motion aligns with cluster members within 3σ . Its proper motion also aligns with members of the OB association no. 15 at a distance of 3902 pc (Chemel et al. 2022). We applied a 0.25 mas yr^{-1} proper motion cut around HD 331777's value on stars within $10'$ of the target. We calculated a group distance of 3789^{+190}_{-176} pc. Using the *Gaia* DR3 radial velocity of $0.8 \pm 5.5 \text{ km s}^{-1}$, we found a H α -based distance in a very wide range of 2000–5000 pc.

RW Cep. The *Gaia* DR3 parallax is medium-quality ($\varpi/\sigma_\varpi = 3.33$), resulting in a distance of 6666^{+1561}_{-1006} pc. The star's proper motion aligns with the open cluster Berkeley 94 at a distance of 4000 ± 40 pc (Hunt & Reffert 2024) within 3σ and it has been identified as a cluster member (Delgado et al. 2013) or a member of the Cep OB1 association (Humphreys 1978). Its proper motion aligns with the OB association no. 122 (Chemel et al. 2022) at a distance of 3876 pc. We applied a 0.1 mas yr^{-1} proper motion cut around RW Cep's value on stars within $10'$ of the target. We calculated a group distance of 3921^{+168}_{-157} pc. Using the radial velocity of $-50 \pm 3 \text{ km s}^{-1}$ (Kasikov et al. 2025), we found a H α -based distance of ~ 3500 pc.

V509 Cas. The *Gaia* DR3 parallax is medium-quality ($\varpi/\sigma_\varpi = 3.96$), resulting in a distance of 3917^{+969}_{-737} pc. It has been identified as a member of Cep OB1 association (Mel'nik & Dambis 2017; Humphreys 1978). Its proper motion aligns with OB association no. 120 at a distance of 3055 pc (Chemel et al. 2022), which has proper motions consistent with

the Cep OB1 association (Mel'nik & Dambis 2017). We applied a 0.4 mas yr^{-1} proper motion cut around V509 Cas' value on stars within $10'$ of the target. We calculated a group distance of $3368 \pm 127 \text{ pc}$. This distance is about 2.5 times larger than the distance of 1370^{+561}_{-398} pc from the *Hipparcos* parallax used by Nieuwenhuijzen et al. (2012). Using the radial velocity of -60.7 km s^{-1} (Kasikov et al. 2024), we found a H α -based distance of $\sim 3800 \text{ pc}$.

6 Cas. The group distance determination for 6 Cas is given in detail in Sect. 3.2. Using the *Gaia* DR3 radial velocity of $-43 \pm 8 \text{ km s}^{-1}$, we found a H α -based distance in the range of 2000–3000 pc.

HD 223767. The *Gaia* DR3 parallax is high-quality ($\varpi/\sigma_\varpi = 20.17$), resulting in a distance of $2879^{+136}_{-117} \text{ pc}$ (Bailer-Jones et al. 2021). It has been identified as a member of Cas OB5 association (Mel'nik & Dambis 2017; Quintana et al. 2025). On the sky, the star is very close to the open cluster King 12 (distance $2805 \pm 19 \text{ pc}$; Hunt & Reffert 2024), but its proper motion is slightly outside of the 3σ radius. Its proper motion aligns with the OB association no. 141 at a distance of distance 2827 pc (Chemel et al. 2022). We applied a 0.2 mas yr^{-1} proper motion cut around HD 223767's value on stars within $10'$ of the target. We calculated a group distance of $2740^{+86}_{-83} \text{ pc}$. Using the *Gaia* DR3 radial velocity of $-41 \pm 2 \text{ km s}^{-1}$, we found a H α -based distance in the range of 2000–3000 pc.

ρ Cas. The *Gaia* DR3 parallax is negative. The star has been identified as a member of the Cas OB5 association (Mel'nik & Dambis 2017). However, we found that the proper motions of the association members differ by $\sim 1 \text{ mas yr}^{-1}$ and the association is located $> 2 \text{ deg}$ away on the sky. We did not find alignment with any known cluster or OB association. We applied a 1 mas yr^{-1} proper motion cut around ρ Cas' value on stars within $20'$ of the target. As there are very few hot stars in the region, we included cooler stars down to 7000 K. Among stars with similar proper motions appear two distinct groups: six stars at 1700–2100 pc (*Gaia* parallaxes between 0.47 and 0.54) and 17 stars at 2500–3500 pc (parallaxes between 0.27 and 0.38). The second group includes three stars with $T_{\text{eff}} > 8000 \text{ K}$, all other stars in both groups are cooler. For estimating the distance of ρ Cas, we used the mean parallax of the second group. We calculated a group distance of $2810^{+104}_{-102} \text{ pc}$. Using the radial velocity of $-47 \pm 2 \text{ km s}^{-1}$ (Lobel et al. 2003), we found a H α -based distance in the range of 2500–3200 pc, in agreement with the distance to the farther stellar group.

Appendix B: Proper motion cuts for group distance determination

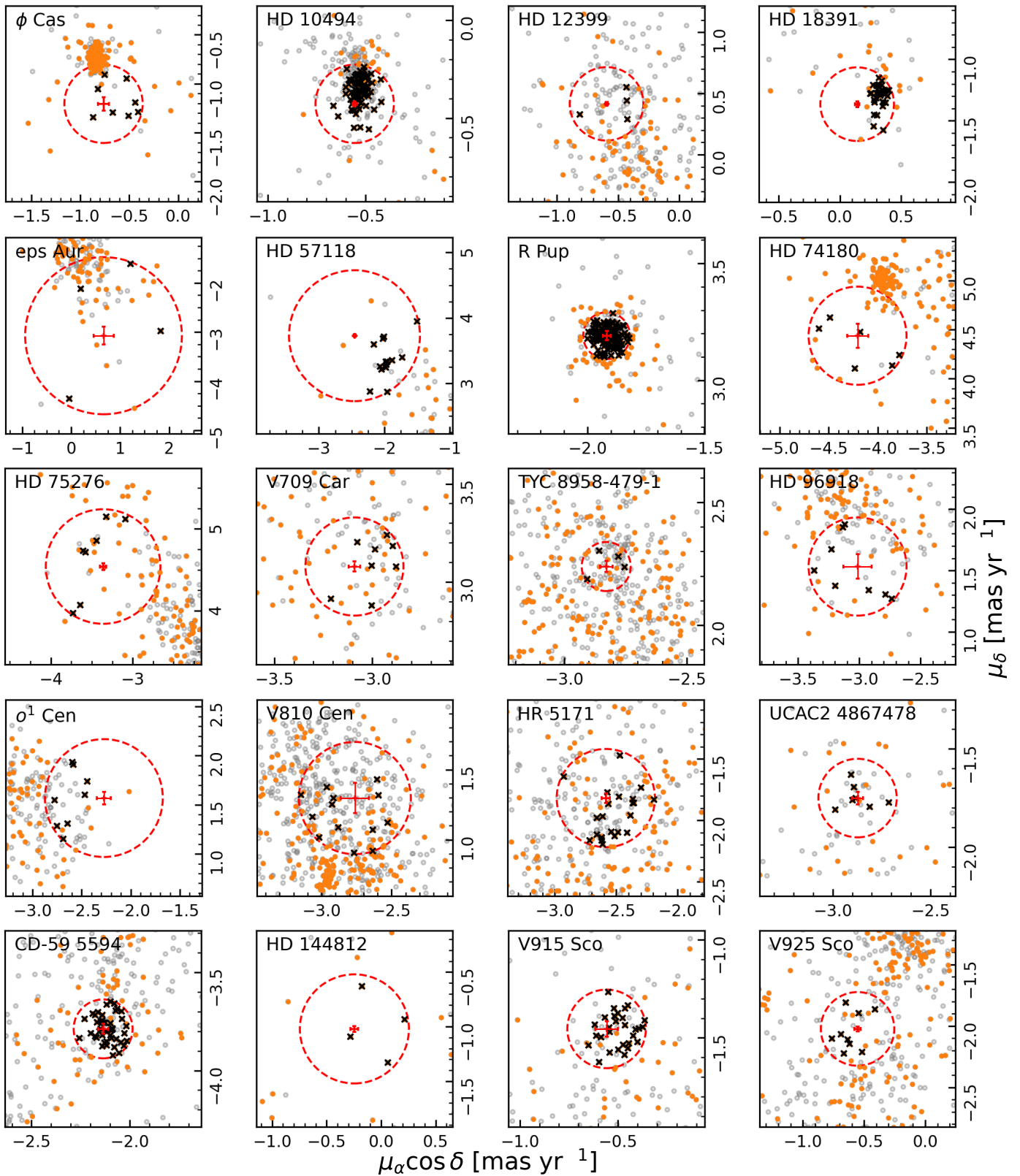


Fig. B.1: Selection of hot stars around each sample YSG/YHG based on proper motion criteria. The YSG/YHG is in the centre with error bars. The red dashed circle marks the proper motion cut radius. Stars shown as orange circles meet the selection criteria from Sect. 3. Stars used for calculating the group distance are marked with black crosses.

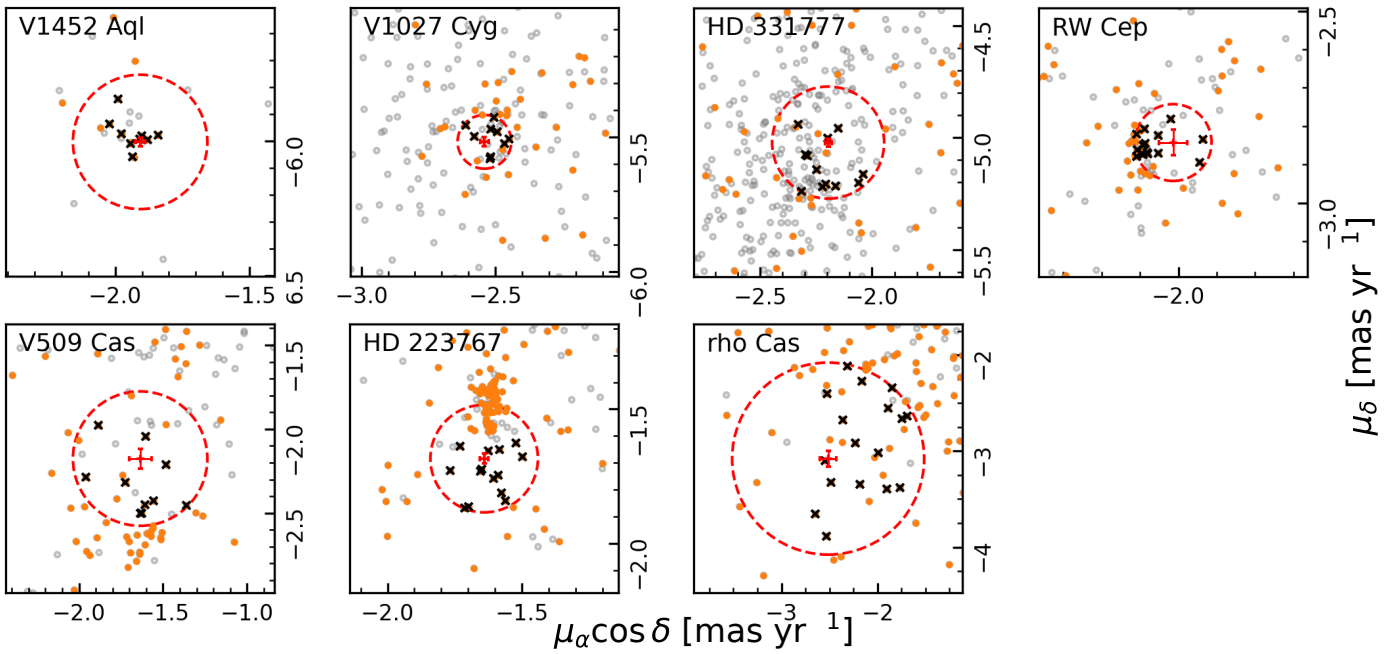


Fig. B.2: Fig. B.1. continued.

Appendix C: Stars selected for group distance determination

Table C.1: Stars selected for the group-based distance calculation. Listed are the relevant *Gaia* DR3 parameters used for proper motion bias and parallax zero-point corrections. The distance from Bailer-Jones et al. (2021) is also included. The table includes the corrected proper motions, the corrected parallaxes and external parallax uncertainties. Shown here are the first three rows for ϕ Cas.

ϕ Cas				
SOURCE_ID	ra	dec	parallax	parallax_error
413874460384818432	19.929	58.243	0.396	0.018
413827043942817792	19.992	58.172	0.361	0.022
413876556328777728	19.972	58.333	0.29	0.02
...				
pmra	pmra_error	pmdec	pmdec_error	phot_g_mean_mag
-0.966	0.013	-1.33	0.014	14.018
-0.835	0.017	-1.191	0.021	14.973
-1.277	0.014	-1.292	0.016	14.645
...				
nu_eff_used_in_astrometry	pseudocolour	ecl_lat	astrometric_params_solved	
1.544	nan	45.135	31	
1.529	nan	45.057	31	
1.574	nan	45.199	31	
...				
pmra_corr	pmdec_corr	rgeo	b_rgeo	B_rgeo
-0.966	-1.33	2353.305	2251.713	2445.136
-0.835	-1.191	2570.845	2431.047	2744.906
-1.277	-1.292	3090.492	2907.08	3318.825
...				
zpt	plx_corr	k_value	plx_ext_uncert	weight
-0.032	0.428	1.498	0.028	0.161
-0.032	0.392	1.403	0.033	0.121
-0.032	0.322	1.436	0.03	0.144
...				

Appendix D: Radial velocities

Table D.1: Radial velocities compiled from the literature. For *Gaia* DR3 values, the errors are 1/2 of the total radial velocity variability amplitude.

Identifier	v_{rad} (km s $^{-1}$)	Ref.
ϕ Cas	-19.2 \pm 3.0	<i>Gaia</i> DR3
	-28 \pm 3	Arellano Ferro et al. (1988)
	-28.5 \pm 1.2	Rosenzweig & Anderson (1993)
HD 10494	-30.6 \pm 1.4	<i>Gaia</i> DR3
	-35 \pm 1	Smolinski et al. (1980)
HD 12399	-44.1 \pm 7.6	<i>Gaia</i> DR3
HD 18391	-38.5 \pm 2.8	<i>Gaia</i> DR3
ϵ Aur	-2.26 \pm 0.15	Stefanik et al. (2010)
HD 57118	61.2 \pm 1.4	<i>Gaia</i> DR3
R Pup	69.1 \pm 4.0	<i>Gaia</i> DR3
	62.5 \pm 0.5	Balona (1982)
HD 74180	25 \pm 3	Forbes & Short (1994)
HD 75276	26.7 \pm 1.2	<i>Gaia</i> DR3
	32.0 \pm 2.5	Reed (2000)
	21.6 \pm 0.47	De Medeiros et al. (2002)
V709 Car	8.4 \pm 8.0	<i>Gaia</i> DR3
	12 \pm 6	Maas (2003)
HD 96918	5.6 \pm 0.5	Balona (1982)
	7.3	Humphreys (1978)
o^1 Cen	-21.1 \pm 9.5	<i>Gaia</i> DR3
	-20.8 \pm 0.6	Gontcharov (2006)
V810 Cen	-16.7 \pm 3.7	Kienzle et al. (1998)
HR 5171A	-40	Humphreys et al. (1971)
	-38	Balona (1982)
UCAC2 4867478	-41.4 \pm 3.6	<i>Gaia</i> DR3
CD-59 5594	-35.7 \pm 4.2	<i>Gaia</i> DR3
V870 Sco	-43.2 \pm 5.5	<i>Gaia</i> DR3
	-53	Herbig (1972)
V915 Sco	-6	Andrews (1977)
IRAS 17163-3907	18*	Wallström et al. (2017)
V925 Sco	-15.6 \pm 5.8	<i>Gaia</i> DR3
	-14.7 \pm 1.7	Kipper (2008)
[FMR2006] 15	102.2*	Figer et al. (2006)
	120.8*	Davies et al. (2008)
IRAS 18357-0604	90 \pm 3	Clark et al. (2014)
HD 179821	85.8 \pm 0.8	Şahin et al. (2016)
V1452 Aql	32.7 \pm 8.3	<i>Gaia</i> DR3
	32 \pm 1.5	Smolinski et al. (1980)
IRC +10420	60 – 68	Klochkova et al. (1997)
	76.2 \pm 1.1*	Jones et al. (1993)
	77*	Oudmaijer et al. (1996)
V1027 Cyg	8.7 \pm 10.3	<i>Gaia</i> DR3
	5.5	Klochkova et al. (2016)
HD 331777	0.8 \pm 5.5	<i>Gaia</i> DR3
RW Cep	-50.3 \pm 3.3	Kasikov et al. (2025)
	-53.3 \pm 4.0	<i>Gaia</i> DR3
V509 Cas	-60.7	Kasikov et al. (2024)
6 Cas	-43.0 \pm 8.4	<i>Gaia</i> DR3
HD 223767	-41.2 \pm 2.1	<i>Gaia</i> DR3
ρ Cas	-47 \pm 2	Lobel et al. (2003)

* v_{LSR} velocity

Table 1: Distances and cluster/OB association memberships for YSGs/YHGs. The targets are ordered by increasing right ascension. 'Stellar group' indicates that the star is not associated with any known cluster or OB association, but a co-moving group of nearby stars is identified.

Identifier	Distance <i>Gaia</i> ⁽⁴⁾ (pc)	Lit. clus- ter/assoc.	Lit. dis- tance (pc)	Ref.	Ident. clus- ter/assoc.	Distance to cl/assoc. (pc)	Ref.	H _I kin- ematic dis- tance (pc)	Group dis- tance (pc)
ϕ Cas	3978^{+1627}_{-903}	NGC 457	2420	5,6	NGC 457	2800 ± 9	2	1000-1800	2920^{+114}_{-113}
HD 10494	2823^{+142}_{-114}	NGC 654	2450	5,6	NGC 654	2815 ± 11	2	1000-1800	2784^{+57}_{-61}
		Cas OB8	2300	7	Chemel 150	2626	3		
HD 12399	3792^{+240}_{-192}	-	-	-	-	-	-	2000-3200	3564^{+320}_{-266}
HD 18391	2263^{+113}_{-93}	Anon.	1661 ± 73	8	SAI 25	2252 ± 11	2	2000-2800	2242^{+49}_{-52}
ϵ Aur	1056^{+218}_{-182}	Aur OB1	1060	5,7	Chemel 143	2262	3		
		-	900	9	Chemel 147	1154	3	~ 700	1127 ± 31
		-	1500 ± 500	10					
HD 57118	2759^{+116}_{-138}	-	-	-	Chemel 25	2524	3	~ 3300	2790^{88}_{-93}
R Pup	3958^{+291}_{-228}	NGC 2439	4450	5,11	NGC 2439	3350 ± 13	2	~ 3500	3331^{+77}_{-80}
		Vel OB1	1460	7,12	Chemel 68	3237	3		
		Vel OB1	1750 ± 156	13	Chemel 107	1935	3	1500-2000	1657^{+33}_{-34}
HD 75276	1443^{+74}_{-57}	Vel OB1	1460	7	Chemel 106	1447	3	~ 1500	1538 ± 24
		Vel OB1	1750 ± 156	13					
V709 Car	4006^{+397}_{-376}	-	-	-	Stellar group		-	~ 3600	3817^{+315}_{-271}
TYC 8958-479-1	8783^{+376}_{-330}	Barbá 2	7390^{+650}_{-550}	14	Chemel 8	6917	3	-	7025^{+687}_{-372}
HD 96918	4583^{+1376}_{-1127}	Car OB2	1790	7	Chemel 210/211/2362/2450	500/5000	3	$500/5000$	2623^{+388}_{-83}
		Car OB2	2000	12					
		-	2700 ± 1000	15					
σ^1 Cen	3783^{+3197}_{-928}	-	-	-	-	-	-	~ 2800	2880 ± 100
V810 Cen	5312^{+2095}_{-1319}	Cru OB1	2010	7	Chemel 205	2347	3	2400-3500	2330^{+61}_{-65}
		Stock 14	2780 ± 120	16	Stock 14	2340 ± 9	2		
HR 5171A	3601^{+649}_{-539}	Gum 48d	3500	17	SFR	-	-	~ 3500	$2953^{+92}_{-96}^{(a)}$
		R 80	3600	12					
		R 80	2900	7					
		-	1500 ± 500	18					
UCAC2 4867478	3327^{+465}_{-331}	-	-	-	Stellar group	-	-	~ 3600	3322^{+351}_{-314}
IRAS 14394-6059	5450^{+770}_{-686}	-	-	-	-	-	-	-	$-\ast$
CD-59 5594	3739^{+325}_{-279}	-	-	-	Pismis 21	2906 ± 24	2	~ 2500	2849 ± 77
		-	-	-	Chemel 47	2958	3		
HD 144812	1352^{+66}_{-58}	-	-	-	-	-	-	-	$1374^{+169}_{-132}^{(a)}$
V870 Sco	3945^{+940}_{-642}	NGC 6231	< 2090	19	-	-	-	~ 3500	$-\ddagger$
		backgr.							
V915 Sco	1717^{+175}_{-115}	-	2630^{+390}_{-339}	20	HSC 2870	2350 ± 25	2	1500-2000	2253^{+57}_{-56}
		-	2800 ± 1100	21	Chemel 82	2250	3		
IRAS 17163-3907	5196^{+1401}_{-1032}	-	1200^{+400}_{-200}	22	-	-	-	~ 1000	$-\ddagger$
		-	$3600-4700$	23					
		RCW 122	3380 ± 300	24					
		-	~ 1000	24					
V925 Sco	3006^{+192}_{-166}	Trumpler 27	2427	25	Chemel 82	2250	3	1800-4000	2310^{+126}_{-110}
		Trumpler 27	2100 ± 200	26					
[FMR2006] 15	3654^{+1743}_{-1750}	RSGC 1	5800	27	RSG group	-	-	~ 6500	$-\ddagger$
		RSGC 1	6600	28					
IRAS 18357-0604	4539^{+1939}_{-1655}	RSG assoc.	~ 6000	29	RSG assoc.	-	-	~ 5500	$-\ddagger$
HD 179821	4432^{+349}_{-355}	-	6000	18	-	-	-	> 5000	$-\ast$
		-	6000 ± 1000	30					
		-	≥ 4000	31					
V1452 Aql	2748^{+193}_{-148}	-	-	-	CWNU 1591	2290	4	2500-3500	2472^{+111}_{-104}
IRC+10420	4260^{+878}_{-752}	-	5800	32	-	-	-	~ 5500	$-\ast$
		-	4000-6000	33					
V1027 Cyg	3723^{+265}_{-237}	-	-	-	Chemel 15	3902	3	2000-4500	3977^{+226}_{-208}

Table 1: continued.

Identifier	Distance <i>Gaia</i> ⁽¹⁾ (pc)	Lit. clus- ter/assoc.	Lit. dis- tance (pc)	Ref.	Ident. clus- ter/assoc.	Distance to cl/assoc. (pc)	Ref.	H ₁ kine- matic dis- tance (pc)	Group dis- tance (pc)
HD 331777	4559 ⁺³⁸⁸ ₋₃₆₃	-	-		Kronberger 54 Chemel 15	4025 ⁺⁷³ ₋₇₀ 3902	2 3	2000-5000	3789 ⁺¹⁹⁰ ₋₁₇₆
RW Cep	6666 ⁺¹⁵⁶¹ ₋₁₀₀₆	Berkeley 94 Cep OB1	3900±110 3470	34 12	Berkeley 94 Chemel 122	4000 ± 40 3876	2 3	~3500	3921 ⁺¹⁶⁸ ₋₁₅₇
V509 Cas	3917 ⁺⁹⁶⁹ ₋₇₃₇	Cep OB1 Cep OB1	2780 3470	7 12	Chemel 120	3055	3	~3800	3368 ± 127
6 Cas	2319 ⁺⁴⁶³ ₋₂₈₈	Cas OB5	2500-3000 2780 ⁺³⁷⁰ ₋₂₉₀	7,36 37	Chemel 141	2827	3	2000-3000	2790 ⁺⁷⁰ ₋₇₁
HD 223767	2879 ⁺¹³⁶ ₋₁₁₈	Cas OB5	2500-3000	7,36	Chemel 141	2827	3	2000-3000	2740 ⁺⁸⁶ ₋₈₃
ρ Cas	6747 ⁺¹¹⁷ ₋₁₆₄₇	Cas OB5	2500-3000 2500 ± 500	7,36 18	-	-		2500-3200	2810 ⁺¹⁰⁴ ₋₁₀₂
			3100±500	38					

Notes. * Use Bailer-Jones et al. (2021) distance. † Use H₁-based distance. ^(a) See comments in App. A.

References. (1) Bailer-Jones et al. (2021); (2) Hunt & Reffert (2024); (3) Chemel et al. (2022); (4) He et al. (2023a); (5) Arellano Ferro & Parrao (1990); (6) Rastorguev et al. (1999); (7) Mel'nik & Dambis (2017); (8) Turner et al. (2009); (9) Strassmeier et al. (2014); (10) Guinan et al. (2012); (11) White (1975); (12) Humphreys (1978); (13) Reed (2000); (14) Maíz Apellániz & Negueruela (2025); (15) Achmad et al. (1992); (16) Turner (1982); (17) Karr et al. (2009); (18) van Genderen et al. (2019); (19) Damiani et al. (2016); (20) Andrews (1977); (21) Vasquez et al. (2005); (22) Koumpia et al. (2020); (23) Lagadec et al. (2011); (24) Wallström et al. (2015); (25) Perren et al. (2012); (26) Moffat et al. (1977); (27) Figer et al. (2006); (28) Davies et al. (2008); (29) Clark et al. (2014); (30) Hawkins et al. (1995); (31) Reddy & Hrivnak (1999); (32) Nedoluha & Bowers (1992); (33) Jones et al. (1993); (34) Delgado et al. (2013); (35) Nieuwenhuijzen et al. (2012); (36) Quintana et al. (2025); (37) Maíz Apellániz et al. (2021a); (38) Zsoldos & Percy (1991)